Addis Ababa University

Addis Ababa Institute of Technology

School of Mechanical & Industrial Engineering

Computational Fluid Dynamics and Experimental Analysis of a Self-Aspirated Domestic Biogas Cook Stove with a Two-layer Porous Radiant Burner to Improve the Performance of Conventional Burner

A Thesis Submitted to the School of Graduate Studies of Addis Ababa Institute of Technology, Addis Ababa University in partial fulfillment for the Degree of Master of Science in Mechanical Engineering (Thermal Engineering)

By: Yared Yalew Temesgen

Advisor: Kamil Dino Adem (Ph.D)

Addis Ababa, Ethiopia
June 2023

Addis Ababa University
Addis Ababa Institute of Technology
School of Graduate Studies
School of Mechanical and Industrial Engineering

Computational Fluid Dynamics and Experimental Analysis of a Self-Aspirated Domestic Biogas Cook Stove with a Two-layer Porous Radiant Burner to Improve the Performance of Conventional Burner

By

Yared Yalew Temesgen

Approved by the Board of Examiners:

Advisor Name	Signature	Date
Internal Examiner	Signature	Date
External Examiner	Signature	Date
Dr. Araya Abera School Dean	Signature	Date
Dr. Sosina Mengistu Associate Director for PG Program	Signature	Date

Declaration

I hereby declare that the work which is being presented in this thesis entitled “Computational Fluid Dynamics and Experimental Analysis of a Self-Aspirated Domestic Biogas Cook Stove with a Two-layer Porous Radiant Burner to Improve the Performance of Conventional Burners ” is original work of my own, has not been presented for a degree of any other university and all the resource of materials used for this thesis have been duly acknowledged.

_____ _____

Yared Yalew Temesgen Date

This is to certify that the above declaration made by the candidate is correct to the best of my Knowledge.

_____ _____

Dr. Kamil Dino Adem (Advisor) Date

Acknowledgment

First, I want to express my enormous thanks to the Almighty God for his continuous and priceless help and permission to finish my graduate study successfully. I want to say that I'm sincere and heartfelt thanks for my advisor, **Kamil D. Adem (Ph.D.)** for his guidance, constructive and stimulating comments, and for his friendly treatment in all the consultations; I had with him during this thesis work. Besides, I would like to say thank you to the School of Mechanical and Industrial engineering, particularly to the Thermal Engineering stream for facilitating my work. My deepest gratitude also goes to my friends who constantly provide me with support, encouragement, and constructive ideas in the course of this thesis work. Finally, I would like to thank my loving family for their endless encouragement and support during the entire period.

Abstract

To meet the requirements of increased thermal efficiency and reduced pollutant emissions of a conventional burner biogas cookstoves, a porous radiant burner (PRB) is added to these conventional burners. The porous radiant burner operates on an excess enthalpy approach, which asserts that recirculates the lost heat from hot combustion products to incoming fuel-air mixture. However, to achieve this excess enthalpy combustion with high reactant velocity, these porous burners employ compressed air, which requires an additional compressor. This thesis aims to investigate the performance of a naturally aspirated domestic biogas stove with a double-layer porous radiant burner cookstove. In the present work, the porous radiant burner comprising silicon carbide (SiC) and cast iron is investigated via numerical and experimental analysis. In the numerical analysis, the geometry of the existing porous radiant burner cookstove is modified with new features such as an orifice and slots (for air entrance) to get higher reactant velocity and lower pressure drop without using an external compressor. Then, the experimental investigation follow-up to evaluate the performance of the new naturally aspirated porous radiant burner, and compared it with the existing conventional burner.

The numerical results indicate that naturally aspirated porous radiant burner has a better pressure distribution and higher reactant velocity than the existing burner and it can be operate without external pumping . The experimental results show that the naturally aspirated PRB has improved thermal efficiency in the range of 51-59%, reduced carbon monoxide (CO) and nitric oxides (NOx) pollutant emissions in the range of 41-55 and 4-10 parts per million at gas flow rates of 6-8 liters per minute, respectively. The new self-aspirated porous radiant burner biogas cook stove has 3.5% improved efficiency, 79.4% CO, and 28.7% NOx lower pollutant emissions compared to conventional burner cookstoves. Finally, this self-aspirated porous radiant burner biogas stove will have better efficiency if the best thermal resisting material is used and utilizes the biogas at a pressure greater than the atmospheric pressure.

Keywords; porous radiant burner, biogas, conventional burner

Table of Contents

List of figures

List of tables

Abbreviation

CB	Conventional Burner
CFD	Computational Fluid Dynamics
CCT	Controlled Cooking Test
CGB	Conventional Gas Burner
CKP	Conventional Kerosene Pressurized stove
CZ	Combustion Zone
GHG	Green House Gases
ICS	Improved Cook Stoves
LCV	Lower Calorific Value
LPG	Liquefied petroleum Gas
LPM	Liters per Minute
NBPE	National Biogas Program of Ethiopia
PIM	Porous Inert Media
PMC	Porous Media Combustion
PPM	Parts per Million
PPC	Pores per centimeter
PPI	Pores per inch
PKP	Pressurized kerosene porous
PMB	Porous media burner
PRB	Porous radiant burner
PRRB	Porous recirculating radiant burner
PZ	Preheating zone
WBT	Water boiling test
WHO	World Health Organization

Acronyms

ϕ	Equivalence ratio
v	Velocity
ρ	Density
C_p	Specific heat
T_f	Final temperature
T_i	Initial temperature
T_g	Temperature of gas
$\dot{m}$	Mass flow rate
$\dot{V}$	Volume flow rate
m_w	Mass of water
h_{ev}	Enthalpy of vaporization
η_{th}	Thermal efficiency
t	Time
Q_{LHV}	The lower heating value of gas
K_f	Thermal conductivity
φ	Porosity
h_v	Volumetric heat transfer coefficient
ω	Scattering albedo
G	Irradiance
η_{rad}	Radiation efficiency
E_b	Planck's black body emitted flux
q	Radiation heat transfer
H_c	Enthalpy of combustion
S_{fg}	Rate of fuel consumption per unit volume

CHAPTER 1
INTRODUCTION

In this introduction section, a brief introduction of the biogas fuel including the process of production, combustion, and flame properties of biogas in different types of burners including the principle of the porous media combustion and materials used as porous radiant burners will be discussed. Next, the problem statement and the objectives of the thesis will be presented, and the scope that this thesis will cover follow up. The significance of the study will be presented and finally, the organization of the thesis will be discussed and summarized.

1.1 Background of the study

Energy plays a crucial role in changing the standard of everyday life of human beings. The worldwide energy demand is increasing rapidly as a result of population growth and economic development (Bildirici & Özaksoy, 2018). Traditional biomass fuels account for about 85% of household energy use in developing countries' rural areas. Primary energy sources for culinary tasks include fuelwood, charcoal, agricultural leftovers, and animal manure (Keles et al., 2017). The World Bank reports, that in Ethiopia about 80% of the population lives in the rural areas with agriculture as the primary source of income. About 88% of these rural households does not have access to electricity and rely on woody biomass, agricultural residue and sundried livestock manure mostly for cooking (Bank, 2018). Such fuels have negative consequences for that directly involved, due to particulate matter concentrations from inefficiently burned fuels and time-consuming fuel collection, as well as for the community, due to ambient pollution from simultaneous cook-fires and land degradation in cases where fuel wood is gathered in an unsustainable manner (Balmes, 2019).

Cooking energy is still a big concern for consumers and policymakers all around the world. Cooking is a common home activity that necessitates a large amount of energy and human work (Castro et al., 2018). The firewood and charcoal produced from the common resource serve as a means of income for poor rural and urban households (Cozzi et al., 2020). To answer the need to address the adverse impacts of the increasing trend in biomass energy consumption, biogas is introduced as an alternative renewable energy. Anaerobic digestion of organic substrates, such as manure, sewage sludge, the organic components of household and industrial waste, and energy crops, results in the production of biogas. It is created in small-scale digesters found globally as well as large-scale digesters first discovered in industrialized nations (Sawyerr et al., 2019). Biogas consists mainly of methane (CH_4) and carbon dioxide (CO_2) and

it can be utilized as a renewable energy source in combined heat and power plants, as a vehicle fuel, or as a substitute for natural gas. Because of this energy release, biogas can be utilized as a fuel for any heating purpose, including cooking (Zain & Mohamed, 2018).

This biogas fuel was used in so many applications such as household cooking fuel, institutional cooking fuel, and internal combustion engines and nowadays it is used as a blending fuel with diesel for different applications. To utilize this biogas in household applications for cooking purposes the fuel will be burned on the stove where the pot would be put on. An enclosed space where biogas is burned to heat either the area where the stove is located or items placed on the heated stove is referred to as a biogas stove. Although there are various varieties of biogas stoves available, the bulk of these stoves is inefficient and expensive (Orhorhoro et al., 2018). Because biogas has a low calorific value (LCV), its quality improvement procedure is costly, and combustion occurs in the free flame mode, resulting in ineffective combustion. Heat transmission is primarily through convection, with radiation conduction modes being negligiable. As a result of these factors, the conventional biogas cook stove burner is less efficient at emitting harmful pollutants into the atmosphere (Devi et al., 2019).

In these, regard to reduce the hazardous emissions and to increase the performance of the conventional biogas burners significant amount of researches has been dedicated for the development of efficient and environmentally friendly combustion techniques. Porous inert burner (PIB) or porous media combustion (PMC) is one such technology that utilizes heat recirculation features of highly conducting and radiating porous matrix (PM) for offering lower levels CO and NOx emissions as well as higher thermal efficiency than the burners operating on the basis of free flame combustion (Mishra & Muthukumar, 2018). The combustion of air fuel mixture with in the PIB helps in stabilizing of flame with in the pore structure of the solid matrix/media. Exhaust products heat the PIB downstream of the flame zone. Some of this heat is then conducted to and radiated back to the upstream section, which preheats the incoming air fuel mixture. The super adiabatic combustion caused by the recirculation of sensible enthalpy from the hot combustion products to the unburnt air-fuel mixture favors complete oxidation of the fuel, which consequently reduces the CO and unburned hydrocarbon emissions, while the low flame temperature in the post flame region of the PIB inhibits the NOx production (Devi et al., 2019). Because of the heat transfer through the combined modes of conduction, convection and radiation with in the PM, low heating value fuels such as biogas be easily combusted with a substantial improvement in burning velocity, radiant output, flammability limit and power density can be attained. Qwing to higher stability range and better

emission characteristics, PIB integrated with thermal devices has been considered as a potential substitute to conventional burners. Because of these unique features, the PMC technology has gained specific importance in recent years (Kaushik, 2019)

In this research, before the process of developing the self-aspirated household biogas stove with a porous media combustion is started, a mathematical design and two-dimensional modeling of the porous radiant burner are drawn using SOLIDWORKS software to perform finite volume analysis on the designed porous radiant burner structure. Materials used in constructing the whole biogas stove conventional burner and porous radiant burner structure is also been identified and assigned in the software to increase the accuracy of the result. CFD analysis is done on the modeling of the porous burner using the simulation functions in ANSYS® software to determine the distribution of pressure, velocity, and turbulent kinetic energy after the flow parameters are added into the simulation. Then the fabrication of a biogas stove and porous burner continued and the experimental analysis is performed.

1.2 Problem statement

From different literatures and reported works, there is a large variation in the thermal efficiency of conventional biogas cook stoves from 45 to 57%. However, the biogas cook stove becomes less efficient, with a poor combustibility limit, minimal power density, and high pollution emission levels. Towards enhancing the existing biogas stove effectiveness, Devi et al. (2019) and Kaushik et al. (2021) proposed highly conducting and radiating PRB instead of perforated metallic burner head in the biogas-cooking stove. Thermal efficiency and emission characteristics of conventional biogas cook stove with Alumina (Al_2O_3) and silicon carbide (SiC) were investigated. The maximum thermal efficiency of 62% were achieved with higher reactant velocity and combustion stability with wide range of equivalence ratio variation. However, to achieve this higher reactant velocity they uses external compressor to compress the air, and it is not affordable and suitable in domestic applications due to the cost expensiveness of the compressor and portability of the equipment. To enhance the performance of conventional biogas cook stove and to make the new forced air supply PRB biogas stove compatible for household application, here this thesis is presented to design, simulate, and perform an investigation on performance analysis of self-aspirated household biogas cook stove with the aid of double layered porous media combustion or porous radiant burner.

1.3 Research Objectives

1.3.1 General objective

The general objective of this research paper is to develop a self-aspirated domestic biogas cook stove to increase the performance of conventional biogas-fueled cook stoves through computational fluid dynamics simulation, fabrication and perform experimental analysis with two-layer porous radiant burners.

1.3.2 Specific objectives

The specific objectives of this research proposal are

- To select and seizing of the porous media burner which is used in earlier research
- To identify the best burner by performing a CFD Simulation of a Porous radiant burner
- To manufacture own aspirated domestic biogas stove consisting of a double-layered porous medium
- To evaluate the effectiveness and performance of the burner with experimental test analysis

1.4 Scope of the Thesis

The goal of this research is to enhance the overall performance of a biogas cook stove using a porous radiant burner material. The design and development process begins with the study of selecting the best porous material, the mathematical modeling of the burner, and the fabrication of a cook stove with the burner. The analysis of performance, surface temperature distribution, and emission will be done consequently. This stove studied in this thesis is limited in geographical scope because it needs an atmospheric condition above 1 bar. The methodological scope of this study is the financial requirement and the material availability to perform different types of analysis with variations of geometrical parameters of the burner. However, in this study, the detailed analysis of the flame property of the gas and stove may not be included.

1.5 Significance of the study

To ensure a secure fuel use plan and to reduce environmental changes clean cooking access has to be delivered to everyone's home in Ethiopia. Despite developing improved, cook stoves that use biogas fuel some barriers such that are improper consecutive investigation on biogas plants, low awareness, and technical limitations the use of biogas fuel can go beyond the purposes of fences in Ethiopia. The finding of this research will reflect the benefit of using

PRB in household cook-stoves for biogas fuels. It will be given a better way to manufacture improved biogas cook stoves in manufacturing industries and energy sectors. It becomes important to contribute to reducing fuel consumption and environmental impacts. It will become an input for further investigations into cook stove design.

1.6 Organization of the Thesis

There are five chapters in this research. The project's broad background, problem statement, general and specific objectives, scope or limitations, and expected outcomes are all detailed in the first chapter. The second chapter is devoted to a thorough review of the research literature carried out on porous media combustion efforts on the design and development of improved cook stoves for different types of fuels and the chapter will end with final thoughts regarding the literature review. The design and development for the porous media combustion biogas cook stove will be done in the third chapter, as well as general material and processes. The performance evaluation will be discussed in this third chapter by simulating and conducting the experimental investigation. The results and findings will be discussed in the fifth chapter, general conclusions are offered along with suggestions for further investigation.

CHAPTER 2
LITERATURE REVIEW

In this section, the detail introduction of the biogas fuel including the process of production, combustion, and flame properties of biogas will be discussed. Next to that, the fuel consumption and development of the conventional burner biogas cook stoves in Ethiopia will be presented and the design principle of such conventional burners and their testing methods follows up. The principle of the porous media combustion and materials used as porous radiant burners are also included in this section. Finally, the related literature associated with computational fluid dynamics and experimental analysis will be discussed and summarized.

2.1 Biogas production and its combustion properties

2.1.1 Production of Biogas

Biogas is a renewable type of combustible gas that originates from the process of bio-degradation of organic material under anaerobic digestion (not needing oxygen) conditions. The biogeochemical carbon cycle includes an important role in the natural production of biogas. Methanogens, which are bacteria that produce methane, are the last in a line of microbes that break down organic matter and release the byproducts of that breakdown into the environment. In this process, a source of renewable energy, biogas is generated. This gas is principally composed of methane and carbon dioxide (Bharathiraja et al., 2018). The approximate composition of biogas could vary according to the experimental and source condition as shown in Table 2-1.

Table 1 Compositions of Biogas (Bharathiraja et al., 2018)

Composition	Symbol	Percentage
Methane	CH	50-75
Carbon dioxide	CO_2	25-40
Hydrogen	H_2	5-10
Nitrogen	N_2	1-2
Water vapor	H_2O	0.3
Hydrogen sulfide	H_2S	Traces

Hydrolysis, fermentation/acidogenesis, acetogenesis, and methanogenesis are the four major processes that produce biogas. Using water to break the chemical bonds between the substances, complex organic matter is decomposed into simple soluble organic molecules. Fermentation is the chemical degradation of carbohydrates in the absence of oxygen by enzymes, bacteria, yeast,

or molds to produce primarily volatile fatty acids and some acetic acid, as well as H_2 and CO_2. The fermentation products are transformed into acetate, hydrogen, and carbon dioxide by acetogenic bacteria in the third step, and methane is generated from acetate and hydrogen/carbon dioxide by methanogenic bacteria in the final process (Raja & Wazir, 2017). Methane has no odor and is nearly invisible in bright daylight. It has a clear blue flame that emits no smoke and is non-toxic. It generates greater heat than kerosene, wood, charcoal, cow-dung chips, and other similar fuels. Methane has a specific gravity of 0.55 when compared to air, a critical temperature of 82.5°C, and a liquefaction pressure of 5000 psi. The combustion air requirement (m3/m3) is 9.33 (Sawyerr et al., 2019). Biogas has an ignition temperature in the region of 650° to 750° C and is roughly 20% lighter than air. It is a colourless gas that burns with a flame that is similar to LPG gas in that it is clear blue. Biogas which is made from cow dung has a lower calorific value of 16.9 Mega Joules (MJ) per m^3 and burns with 50-60 percent efficiency in a conventional biogas stove(Eriksson, 2010).

2.1.2 Biogas Combustion

In the combustion analysis of biogas, Methane which has the highest volume in biogas combines with oxygen in the air to start a chain of reactions that primarily and preferentially results in carbon dioxide and water, both of which are saturated compounds (those with a net zero valence number). H_2, O_2, N_2, NO_2, OH, and CO are additional substances that are produced in substantial amounts (Marchese, 2015). Since chemical equilibrium involves a statistical distribution of the essentially limitless variety of carbon, hydrogen, and oxygen molecular configurations, these are just a few of the products. The following reaction summary can be used to explain the standard methane combustion in air. The mole fractions of each product depend on temperature, pressure, and intermediary reactions, as the one for water creation in the example below.

H_2O formation;

$$\frac{1}{2}O_2 + H_2 \leftrightarrow H_2O$$

Reaction Summary;

$$CH_4 + 2(O_2 + 3.76N_2) \rightarrow \dot{n}_{CO_2}\, CO_2 + \dot{n}_{H_2O}\, H_2O + \dot{n}_{NO_2}\, NO_2 + \dot{n}_{N_2}\, N_2 + \dot{n}_{H_2}\, H_2 + \dot{n}_{O_2}\, O_2$$

The stoichiometric molar ratio of air and biogas is 5.70 to 1, with an average methane concentration of 60 moles percent in biogas and oxygen content of 21 moles percent in air.

$$\frac{1 \text{ mole ofmethane}}{\text{x mole of biogas}} = \frac{0.6 \text{ mole ofmethane}}{1 \text{ mole of biogas}} \rightarrow 1.6\text{mole of biogas}$$

$$\frac{2 \text{ mole of oxygen}}{\text{x mole of air}} = \frac{0.21 \text{ mole of oxygen}}{1 \text{ mole of air}} \rightarrow 9.52 \text{ mole of air}$$

$$\frac{\text{moles of air}}{\text{moles of biogas}} = \frac{9.52}{1.6} \rightarrow 5.70$$

2.1.3 Flame Type

According to the literature by Zeng et al. (2018), in domestic burners, biogas can burn through diffusion or only partially premixed flames. Flame liftoff is a problem with biogas combustion in both scenarios. When the velocity of the gas and air mixture leaving a port is faster than the laminar flame speed, flame liftoff occurs, and a flashback occurs when the opposite happens. Biogas burners have a higher tendency to lift off because the fuel contains a lot of inert gas (carbon dioxide), which slows down the flame. As a result of incomplete combustion during flame liftoff, carbon monoxide, and unburned hydrocarbon emissions rise, and efficiency declines. Non-premixed fuel can experience significant oxygen inrushes or over-ventilation in the reaction zone, which can prolong the flame and extend the stoichiometric mixture front. Such stretching reduces the laminar flame speed and reaction rate, increasing the likelihood of flame lift. Due to the dominance of soot generation and subsequent annihilation in the reaction zone over the presence of excited C2 and CH radicals, diffusion flames have a yellow hue. Black smoke is produced as soot escapes the reaction zone. Fuel is mixed with some of the stoichiometric oxygen demand from an entrainment effect before the reaction zone, which results in partially premixed flames. An induced decrease in pressure following the injector is what causes the entrainment effect. Premixed flames have a smaller reaction zone than diffusion, which causes a higher reaction rate or rate of reactant consumption. Higher reaction rates result in faster-burning flames and less flame lift. Premixed flames have a blue-green or violet hue because of the stimulated species' chemiluminescence (C2 and CH radicals).).

2.2 Biogas Fuel Consumption in Ethiopia

Cooking is mostly done with polluting fuels and technologies in about 88% percent of Ethiopian rural households, primarily firewood, and it is nearly 100 percent in rural regions. Even though urban households utilize less harmful fuel and technology, they nevertheless rely heavily on biomass: 38% firewood and 30% charcoal. About one-fourth of residences in metropolitan areas employ clean fuel and technology, with 23% using electricity and 1% using liquefied petroleum gas to cook (LPG). Traditional biomass supplies, on the other hand, are becoming limited in Ethiopia, where rising population pressure, deforestation, land degradation, and soil nutrient mining continue to jeopardize energy and food security (Beyene et al., 2018).

Since the introduction of biogas as a fuel in Ethiopia, the National Biogas Program of Ethiopia (NBPE) has been in place since 2009, with three phases: National Biogas Program of Ethiopia Phase I (NBPE-I) from 2009 to 2013, intending to install 10,000 biodigesters and achieved 8161 digesters. From 2014-2019, the Ethiopian National Biogas Program Phase II (NBPE-II) has been in operation. The program aimed to distribute 20,000 high-quality biogas installations through a market-driven distribution model, giving households access to clean energy for cooking and lighting. The initiative will run until March 2019, and an additional 12,585 bio-digesters will be installed under this program alone until February 2019. In April 2017, the Biogas Dissemination Scale-up Program (NBPE+) was established to assure the continuation, scaling-up, and expansion of the efforts and successes accomplished under NBPE-I and II by building an additional 36,000 digesters. More than 58,000 household-sized bio-digesters are being built in eight Ethiopian areas under the NBPE-I, NBPE-II, and NBPE+ programs till April 11, 2019. Though private sector development is still in its infancy, the market is rapidly developing (Ethiopia, 2019).

Household biogas improves living circumstances for everyone, especially women and children, and has an immediate positive impact on plant harvest by reducing the need for traditional fuel sources, increasing access to clean energy, reducing labor requirements, and improving health. According to the NBPE report, at the end of the second phase, over 80% of the initial bio-digester installation target had been met. The number of bio-digester installations grew over time as the phases of deployment progressed (Tajebe, 2016). Cow dung is used as the primary feedstock in all NBPE bio-digesters, with toilet waste as a secondary feedstock. Adopting households experienced a variety of benefits, including improved sanitation and health, particularly for women and children, reduced time spent collecting biomass from fields and forests, reduced household chores for women and children, improved conditions for schoolchildren who can now read for longer hours in the evening, and lower costs for chemical fertilizer purchases (Sime et al., 2020).

2.3 Design Principle of Improved Cook-stoves

The design of improved cook stoves requires both engineering and non-engineering principles, therefore making it more complex than just a piece of ordinary equipment (Berko, 2018). Dr. Larry Winiarski's methods are used to create superior cookstoves in general. These design ideas focus on ensuring clean combustion and maximizing heat transfer by insulating the fire with lightweight and/or heat-resistant materials. Between the fire and the pot, there must be some spacing or distance, which increases the draft and heats the fire. A small amount of draft

produces a lot of smoke, whereas a large amount cools the fire. The amount of fuel added to the cook stove determines the intensity of the fire (Bryden et al., 2005). Design strategies can generally be to have a large surface area for the heating medium and an increased velocity of hot air. The energy that is obtained from open fires is about 90%, but only 10% - 40% of the released energy is transferred to the pot (Belino et al., 2015). As a result, it's critical to remember that heat transfer and combustion efficiency are far more crucial factors in determining the cook stove's total efficiency. Between the cook stove and the bottom surface of the pot being heated, small apertures can be constructed. As a result, less cold air will enter the fire, and less fuel will be used. The study suggests that broader pots with greater diameters provide good heat transfer to improve fuel efficiency (Bryden et al., 2005).

2.4 Testing and Assessment of Cook Stoves

2.4.1 Water Boiling Test

Trade-offs are a part of all standardized examinations. A test's ability to identify minor changes improves when settings are tightly controlled and variability is minimized. A more controlled test, on the other hand, is generally less reflective of actual cooking. The water boiling test is a typical laboratory testing methodology that is meant to deliver reliable and reproducible outcomes. The Water Boiling Test was created to evaluate stove performance in a controlled environment. Therefore it is likely to be less like local cooking than other experiments (International). The primary factors that are checked during the test are the time it takes to boil the particles in the pot, thermal efficiency, specific fuel consumption, burning rate, firepower, and turn-down ratio. WBT is affected by temperature changes and water mass loss in a pot. Although the WBT is an effective tool for the reasons stated above, it is vital to keep in mind its limits. It stimulates the cooking process and is carried out by professional technicians under controlled settings. Even if efficiency and emissions were assessed in the same method for both WBT and CCT, laboratory test findings may differ from results achieved when cooking real items with local fuels (Lombardi et al., 2017).

2.4.2 Controlled Cooking Test

Stoves must be tested under real-world conditions to validate desired effects (such as fuel economy, smoke reduction, or other effects). Controlled tests are useful for comparing various technical aspects of stove design and pre-field performance evaluations. While lab studies allow for differences across stoves, field tests provide a better indicator of performance in real-world situations. Stove testers can use the Controlled Cooking Test (CCT), which was created in

parallel with the WBT, to learn how stoves work with local cuisine, cooking habits, and fuels. Although the CCT is still a lab test, it is carried out by preparing a standardized version of a local meal (Bott, 2014).

2.5 Construction of Biogas stove

The essential components of a biogas stove were the burner head, frame, and injector, as well as the mixing tube, burner pots, and primary air control valve. A biogas plant or a gas container was used to power the stove. The gas flows from the digester to the stove; the pressure in the gas plant or container, as well as the pipe diameter, affects the gas flow rate. With the help of the jet at the burner's input, the speed of the gas is enhanced, creating a draft that pulls air into the pipe. Figure 2-1 shows the design diagram and components of the stove, and the main components are the legs (1), injector (6), mixing tube (5), burner cap (2), support frame (3), gas intake pipe (4), and air control valves (7) (Awulu et al., 2020).

Screwing the injector into a hole drilled in the valve keeps it in place. The injector becomes a nozzle that enters the air-gas mixing chamber. The burner cup or head opens into the Airgas mixing chamber, where the gas can be ignited. The injector and air control valve combine to allow biogas from the gas intake pipe into the mixing chamber at speeds that cause pressure dips in a venturi vacuum effect. As the injector goes in and out of the mixing chamber, this creates regulated air suction at the air-control valve. In the mixing chamber, the entered air (primary air) is entrained into the gas stream to generate an air-gas mixture. The biogas and the incoming air must be thoroughly combined. This occurs as a result of the pipe being extended to a maximum diameter that is proportional to the width of the jet. By widening the gap further, the gas flow rate is again reduced as the diffuse gas flows to the burner head. The gas then needs more oxygen for final combustion which is supplied by the surrounding air (Awulu et al., 2020).

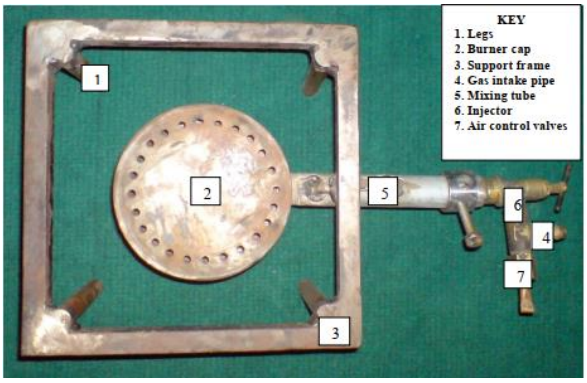

Figure 2-1 Plan view of constructed Biogas Stove (Awulu et al., 2020)

2.6 Porous Media Combustion

Porous medium combustion (PMC) is a self-organized heat recovery and combustion process in porous media that differs significantly from homogeneous flames. The following primary causes are responsible for the disparity. The first factor is that the solid porous medium's inner surface is highly developed, resulting in efficient heat transfer between the combustible medium and the inert solid; the second factor is that dispersion of the reactant flowing through a porous medium increases efficient heat transfer and diffusion between the phases. As a result, an internal energy recovery system is engaged. With the use of this technique, combustion stability can be achieved for a wide range of reactant speeds, oxidant-fuel ratios, plus power loads. The possibility of NOx and CO formation will decrease as combustion efficiency improves (M Abdul Mujeebu et al., 2009). A porous material has linked voids and allows the flow to easily pass through it. The heterogeneous interaction between two distinct media, usually a solid and a gas, is known as porous media combustion (PMC)(M. A. Mujeebu et al., 2009).

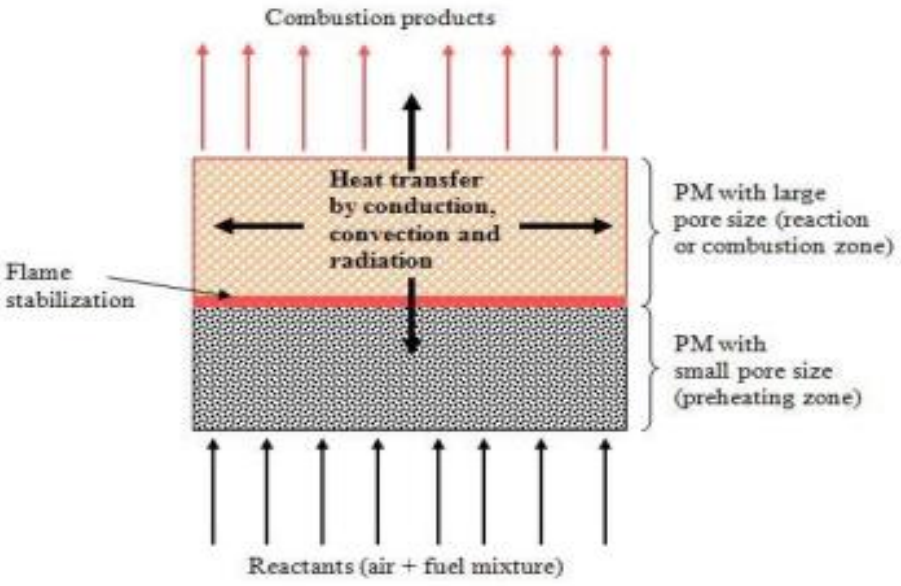

Figure 2-2 Schematic of a two-layer porous burner(M. A. Mujeebu et al., 2009)

The two basic design approaches usually used in PMC are stationary and transient systems. The first technique (stationary) is extensively utilized in radiant burners and surface combustor-heaters because the combustion zone is stabilized in the finite element of a porous matrix by enforced boundary constraints and there is no flame propagation due to the high radiant emissivity of the solid. The 'excess enthalpy' flame theory is based on the second (transient) approach to PMC, in which an unstable reaction zone has the freedom to propagate as a combustion wave in either the downstream or upstream direction due to positive and negative

energy fluxes. Filtration combustion is another name for combustion within a porous inert medium (PIM) (A. K. Ismail et al., 2013). The circulation of thermal energy from combustion-generated products raises the combustion temperature, resulting in a reaction zone enthalpy that is higher than that of conventional combustion. As a result, the phrase "excess enthalpy combustion" has been coined. By utilizing high reactant velocity, this concept can be used to create compact, low-cost, ultra-low-pollution reactors with very high yields. Because the media are inert, they can be used with virtually any type of feedstock. PMC can be used in gas turbines, IC engines, combustion of low-heating-value gaseous fuels like producing gas, heat exchangers, district and room heating, baking ovens, and a variety of other applications (Malico & Mujeebu, 2015).

2.6.1 Heat transfer in PMC

Flames in porous media have higher burning velocities and leaner flammability limits than open flames. These effects are the consequence of a phenomenon named "excess enthalpy combustion" where the heat that is generated in the combustion zone is transferred by radiation and conduction through the solid matrix to the unburned gases. Conventionally, multiple heat flows have been thought of as contributing to the transport of heat through a porous media, including thermal conduction along the solid matrix, thermal radiation across internal pores, and either thermal convection by or conduction by gases filling the pores. Convective heat transfer is inhibited within pores smaller than around 10 mm in gas-filled pores, and this is concerning the latter inevitable selection between convective and conductive heat flux (Kang et al., 2019).

2.6.2 Materials used in PMC

The porous medium can be made from metal, ceramics, plastic, or any material. However, only high-temperature resistance materials such as metal and ceramic are suitable to be used as a medium of combustion. The selection between porous metal and ceramics materials is based on the application of the burner. Metallic materials have less thermal stability and high thermal inertia. Thus, metal porous materials were less used for porous medium combustion. In porous burners, porous ceramics are utilized more frequently than metals because they produce temperature stability during burning with relatively low emissions (A. Ismail et al., 2018). Some of the materials and their properties are summarized in the next table.

Table 2 Summary of Ceramic materials and their thermos-physical properties (Kaushik, 2019)

Materials		Sic	Al2O3	ZrO2	SSic	SiSiC	HPSiC	Cordierite	Mullite	FeCrAl
T_{max}		1600	1900	1800	1400-1700	1380	1700	-	-	-
$K_{cramics}$		20-50	5-6	2-4	40-120	110-160	80-45	2.6	0.37	0.13
ε at 2000 K		0.9	0.28	0.31	-	-	-	-	-	0.65
$\alpha_{th,ex}$20-1000 (10^{-6} k^{-1})		4-5	7.2	10-13	-	-	-	-	-	-
Cp @ 25-800 C		-	1.05	0.59	0.84	0.84	0.84	0.8	-	0.432
T	10 ppi	-	-	28.2	-	-	-	-	-	-
	65ppi	-	-	300	-	-	-	-	-	-
Ω	10ppi	0.55-0.88		0.87-0.99	-	0.7	-	0.76	0.84	-
B	10ppi	234.1	-	-	-	-	-	-	-	-
	20ppi	468.1	210	234	100	178	-	270	202	234.1
	25ppi	585.2	300	-	-	244	-	-	-	-
	30ppi	702.2	-	-	-	-	-	-	-	-

2.7 Development of Biogas Stove in Ethiopia

Biogas cook stoves are attractive in places with wood scarcity. Because to the readily accessible fuel, they completely replace the usage of wood or charcoal and are particularly viable in agricultural areas. The government of Ethiopia and SNV started cooperations to build digesters in the rural parts of Ethiopia. The SNV were manufactured and distributed the number of biogas stoves for domestic cooking. Beside that in Jima University (JU) there were a development and fabrication of biogas stove for Areke distillation. In Ethiopia, *injera* baking represents around 50 to 60% of the households' energy consumption. It was revealed that isolated local research efforts have been conducted to integrate biogas with improved *injera mitads* (or "injera ovens"). The biogas-fueled injera baking oven produced by Et-Solar Tech PLC, which is commercialized as *"Magic Mitad"* and by some of the educational centers like AAU (AAIT) and other univercities across the country. The Magic Mitad substitutes the clay material that is used by traditional mitads with glass. Furthermore, given the fact that injera baking is highly demanded by biogas users, and due to this so much research and developments on biogas stoves are done in the country with governmental and non-governmental institutions (Forn et al., 2014). Institutionally, There are about 235 biogas stoves with a total of 270 pot-holding capacity seats used in different institutions for cooking and baking too. 16 different types of stoves were in use. Currently, the total number of biogas stoves in use is about 148 in 176 potholders. Here it does not include the specially modified appliances used to boil more than 1000litre water mostly

24 hours a day, 7 days a week. One of the institutions (Alema Farms; found in Debrezeit) has been using a unique stove to boil about 10,000liter water daily for a purpose of chicken feather processing(Leta, 2009).

(a) For preparing sauce (by SNV)

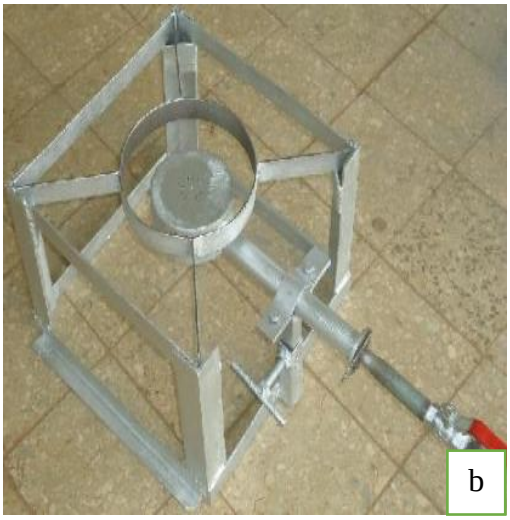

(b) For Areke distillation (JU)

(c) For Injera baking (by AAIT)

Figure 2-3 Biogas stove manufactured in Ethiopia

2.8 Related Work Literatures

In this section, numerous articles related to biogas stove development, CFD analysis of porous radiant burners, and experimental studies on biogas and LPG-fueled stoves with porous radiant burners are reviewed in detail. The purpose of this review is to use as the main starting point for the design development of the porous burners and, this shows where the performance of the newly developed biogas stove will be laydown as a comparative instrument.

The study by Mulugeta et al. (2017) focuses on the design and optimization of an improved biogas injera baking burner for uniform heat distribution of the burner throughout the backing pan. Design and optimization of the burner were employed through analytical and computational fluid dynamics (CFD) simulations of the burner by varying the number and size of flame ports to increase the diameter of the manifold before actual fabrication. To get optimum cooking heat distribution of the injera baking pan the burner's optimum size, the number of holes on the burner, proper mixing of air, and fuel flow rate were analyzed in this study. The conclusion and recommendation made from the results are that the ideal burner manifold diameter is 26 cm can be used to fix the problems of the existing biogas burner for injera baking purposes, due to its ineffective size, the baking pan's heat distribution was uneven throughout due to the external manifold's 17-cm diameter. From the findings, with the best insulation material the 26 cm manifold burner can be used to make the actual hotel size injera with uniform heat distribution throughout the pan.

To deliver sustainable and energy-efficient cooking stoves for Injera baking applications at the domestic and community level Kebede and Kiflu (2014) attempted to design of biogas stove with insulated material to cover the flame. Throughout the process and based on the energy demand needed during the baking process, the amount of gas to be supplied is determined before design. The analysis is performed to ascertain how much heat is transferred from the burner to the baking pan through convection, conduction, and radiation. The data is collected to see how the temperature is distributed through the baking pan and to find the dimension of the pan, and the amount of Teff flour and water to make the dough. The detailed design of the burner is carried out using a mathematical calculation to specify the optimum size of the burner for the required application. From the results obtained from the study, a new burner having a fuel consumption rating of 0.93 m^3/hr, having an insulation material prepared from different materials which have a good insulation property for community-level baking were designed with an approximated baking time compared with existing biomass-fueled Injera baking pans.

Besides using the biogas stove for food making process, Demissie et al. (2016) made a study to utilize the biogas stove for processing and production of alcoholic beverages such as local liquor (‘Areke’) in a district called Arsi Negele, Ethiopia. Through this study, analytical designing of the biogas stove for minimum gas consumption and high efficiency, fabrication, and experimental testing is done depending on the amount of biogas energy needed for the distillation process of Areke. The experiment is carried out using two testing methods called the water boiling test and the control cooking test. The Water Boiling Test (WBT) was used to

evaluate the stove's overall efficiency, which was determined to be 54.8% at the greater flame intensity and 43.6% at the significantly lower flame intensity, respectively. The stove showed a remarkable reduction in the time taken for distilling a pot of distill and which is nearly half of the time it took to distill a pot of distilling using wood. The new stove uses only 0.994 m3 of biogas, compared to 2.088 m3 for the previously tested biogas stove, which is a typical biogas stove for everyday cooking. This study demonstrated that by eliminating 32, 763.70 tonnes of GHG emissions yearly in Arsi Negele alone, the dependence on fuel wood may be reduced by 27.7% if sustainable biogas energy development is undertaken.

Apart from the local research on biogas stoves in Ethiopia, to mitigate the problems associated with heat loss and high biogas consumption by locally manufactured burners, in Tanzania, Petro et al. (2020) researched a novel residential biogas burner's theoretical and experimental performance. Mathematically, the burner's analytical design is carried out, and the development of a jet with a 100 mm manifold burner and an ideal hole diameter of 2.5 mm is made. SOLIDWORKS was used for the 3D modeling of the burner, and Ansys Fluent was used for optimization with computational fluid dynamics (CFD) analysis. This allowed for testing the temperature distribution in the mixing tube and manifold before fabrication by varying the number of flame portholes, air holes, and jet size. The fabrication of the burner is done and the water boiling test is conducted with a cold and hot start at higher power, lower power, and simmering test. The newly created biogas burner and the other two locally produced burners underwent testing and comparison. The water-boiling test (WBT) results then revealed that the developed burner has a thermal efficiency of 67.01% compared to the previously produced Center for Agricultural Mechanization and Rural Technology (CARMATEC) and Simgas burners, which are made in Tanzania, which have thermal efficiencies of 54.61% and 58.82%. Also, the produced burner consumed 736 g/L of fuel as opposed to 920 g/L for CARMARTEC and 833 g/L for that Simgas. Environmentally friendly and cost-effective for household usage in Tanzania and other developing nations, the created hob and its associated cook stove.

To show how the numerical modeling and CFD simulation of porous radiant burners goes on, Tierney et al. (2009) and his friends examine convective and radiative heat transfer models using the commercial computational fluid dynamics (CFD) code ANSYS CFX, to describe the interaction between the porous solid and the fluid. Which incorporated the Navier-Stokes equations, solid and fluid energy equations, and chemical species transport equations. In this study, a 240 mm long SiC foam with 81% porosity is used as a PRB. Ultra-lean CH4/air mixtures were examined at an inlet temperature of 700 K using this model with a 10 atm skeletal

chemical mechanism. The analysis is done in four different cases under the condition of varying the firing rate and the methane concentration in the gas mixture. Super-adiabatic combustion was observed at a firing rate of 200 kW/m2 for CH4 concentrations of 2.00% and 2.25%. The temperature distribution along burner length for all gas mixtures is similar in the temperature profile. The entry zone solid phase is hotter than the fluid phase because of internal heat recirculation from CZ. The result shows fluid temperature becomes higher than adiabatic flame temperature when the firing rate is increased. This is happened due to the heat recirculation from the combustion reaction zone via a solid matrix and is used to preheat the incoming gas mixture. The model results indicated that the energy balance of the system determined the combustion performance and flame location. This balance was directly influenced by heat recirculation within the solid matrix and by solid-to-fluid convective transport.

To study the heat transfer behavior of PRB-assisted LPG-fueled cook stoves for domestic cooking applications Soma et al. (2018) conducted studies on CFD assessments of porous medium burners for use in home cooking. The combustion behavior of a domestic cooking stove has been tested numerically and experimentally by introducing a two-layer porous material and an LPG fuel source.

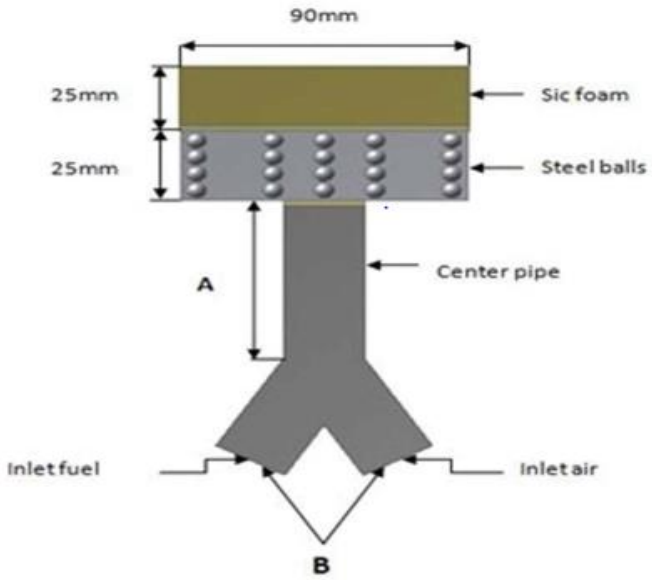

Figure 2-4 Schematic of the two-layer porous medium burner. (Soma et al., 2018)

The PRB material is made of two sections combustion zone with a thickness of 25mm SiC having 10 ppi and a preheating zone filled with steel ball having a thickness of 6.5 mm. The analysis is carried out by varying fluid inlet diameter and the center pipe length with a mass flow rate of 0.05 and 0.009 Kg/m3 and the inlet temperature of the air is 300 K and fuel at 285 K. In this study, a 5% turbulence intensity factor is taken at all inlets and outlets. From the CFD

simulation results, it is observed that a maximum temperature of 2246 K from a porous media burner model has a center pipe diameter of 27.5 and 25 mm. From the analysis, if there is an increase in center pipe length and diameter by half there will be some surface temperature drop. Also, increasing the center pipe length will increase the chance of a flashback.

Jia et al. (2018) Made a new burner and did a numerical simulation on a newly developed Porous medium burner with two sections named preheating and combustion sections and double decks with gas inlets at both ends. The preheating and combustion sections have a length of 0.12 and 0.1 m and they are made of SiC, and the burner is composed of double decks both of which are composed of two porous mediums with different porosities. The analysis is done based on the combustion mechanism of methane/ air mixture in a porous medium and preheating effect. The equations are discretized and solved using fluent software by setting the inlet temperature to 1600 K, standard K-ε model is used for simulation.

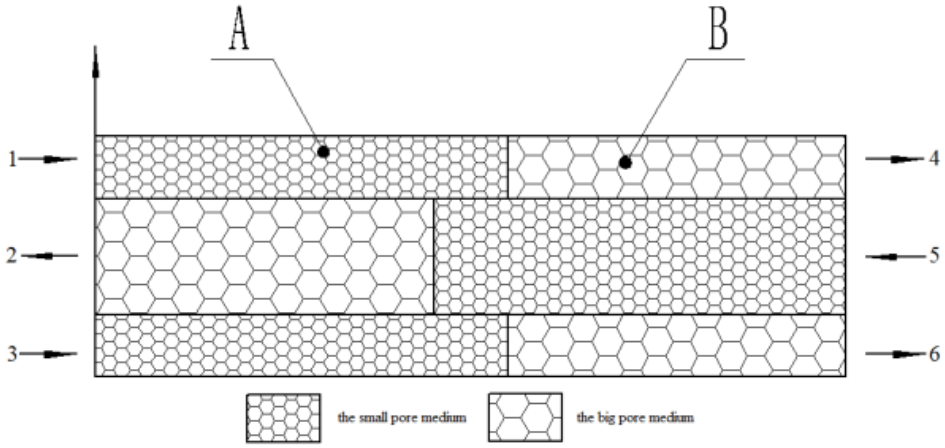

Figure 2-5 Sectional view of the physical model of the new burner (Jia et al., 2018)

When the equivalence ratio is 0.65 and the flow velocity in the inlet is 0.85 m/s, the temperature peak value in the ordinary burner reaches about 1900 K, and the temperature in the outlet is about 1850 K. However, under the same condition, in the new burner, the peak temperature becomes reach about 2600K and in the outlet zone higher than 2400 K. which indicates that premixed gas combustion in the new burner is carried out more thoroughly, and the heat storage and heat transfer capacity of the porous medium in the new burner can be better realized. When the equivalence ratio is 0.85, the inner temperature of the new burner can reach 2700 K. However, the outlet temperature is not less than 2000 K, which is higher than the temperature peak in the ordinary burner under the same conditions. The change in flow velocity of the premixed gas in the inlet exerts an important influence on the combustion in the porous medium. In the case of low flow velocity, the temperature in the inlet increases significantly. The

emission concentration of major pollutants (NOX) from the new burner is much lower than the minimum standard ((100 ppm) in Beijing, China).

Abdulkarim et al. (2019)And their colleagues use CFD to investigate the internal flow of a porous radiant burner, to introduce a metal porous burner design. A metal, cylindrical, two-staged, homogenous porous burner was built based on field experience with porous burners. To lay forth research aspects for porous burners and porous media, the literature was studied. For Combi-boilers and boilers, a three-dimensional solid computer model of a porous metal matrix burner was designed. The design is cylindrical and has an internal structure that allows the fuel to be mixed before combustion. The porosity is uniformly distributed and homogeneous. The flow domain was created from the solid model for use in CFD analysis. Using a commercial computational fluid dynamics code, the flow domain was examined. The estimated flow conditions for the burner were used to run the CFD algorithm. The outcomes were evaluated in terms of the distribution of homogenous flow and flow mixing at the surface. Quantitative data is gathered and provided in the form of contour maps in this study. According to the findings, the porous medium creates a very low-pressure drop, implying a low pumping power need, which is both an advantage and a disadvantage in earlier designs. Although the burner has homogeneous porosity in the axial direction, future research can look at a gradient rise in porosity size toward the inlet. The static and total pressure and velocity magnitude maps are used to calculate it. Total enthalpy increases by 0.02 J/kg. In terms of safe functioning and avoiding self-ignition, this alteration is acceptable. Due to boundary effects and mixing nearby, turbulence arises along the interface walls. The largest quantity of turbulent kinetic energy is around 0.03 J/kg.

Jugjai and Sanitjai (2007) created the first PRB and PRRB for use in household cooking applications to improve the thermal performance of regular or traditional burners by applying porous medium technology. In PRRB, the heat feedback process transfers some gas enthalpy to a premixed mixture via a porous medium, which is act as an emitter or an absorber due to its increased emissivity and high area of coverage to volume ratio. The PRB comprised of porous ceramic material and ran on LPG fuel at a pressure of 0.14 bar with a range of 1 to 3.5 KW of combustion rate. From the experiment, the results of the water boiling test the thermal efficiency of the standard burner varied from 52-56% depending on the increase of combustion rate, and for PRB efficiency become 59-65%. The CO emission from the standard burner at a lower combustion rate is 4-5 ppm and at 2.5KW combustion rate, it is obtained 153-2980 ppm, and in

the case of PRB CO, emission was 3000-3500 ppm due to improper mixing of combustion flame and secondary.

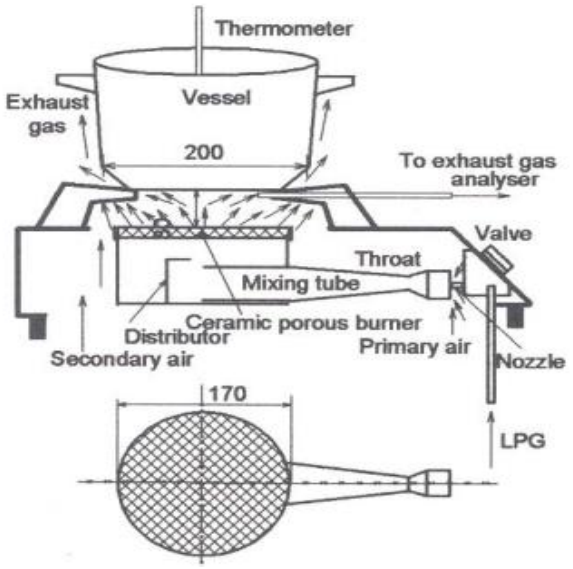

Figure 2-6 Testing of a domestic LPG cooking stove with PRB by Jugjai and Sanitjai (2007)

The values of NOx were found to be 4-22 ppm for PRB and 22-102 for SB, which is considered a lower value In the context of PRB, lower flame temperature, and less extra air are related.

The newly designed a 4 KW combustion rate PRRB is found that has a greater primary air temperature of 210 C with increased thermal efficiency when compared with both SB and PRB.

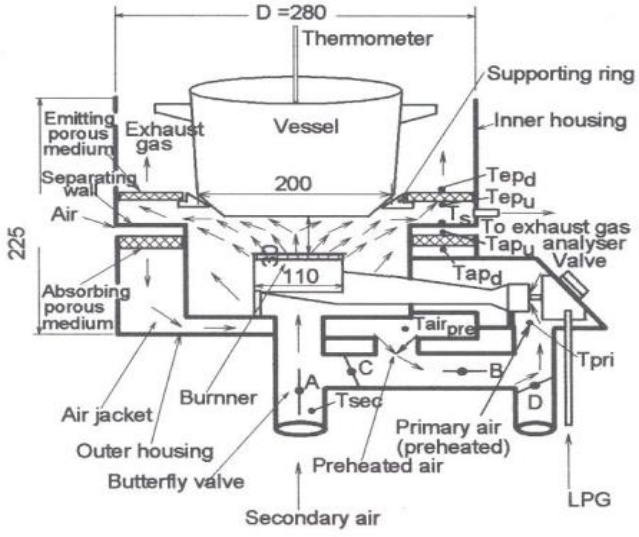

Figure 2-7 Tested PRRB aided LPG cock stove by Jugjai and Sanitjai (2007)

However, there were some drawbacks that an increase in CO emission while considered as constant in PRB. Moreover, in PRRB there is a sharp in increase of NOx when it operates at higher flame temperature as the combustion rate increases. PPRB can generate efficient heat

recirculation and leads to an improvement in the thermal efficiency of domestic cooking stoves. LPG performance in the domestic market Experiments was carried out by Pantangi et al. (2007) putting porous material in the mixing chamber of traditional cooking stoves, including metal balls, pebbles, and metal chunks to improve the thermal efficiency of residential LPG cooking stoves. With and without the use of several types of porous media, thermal efficiency, emission, and energy cost assessments were conducted. There are two zones in the matrix stabilized porous burners. The preheating zone is made up of materials with low porosity and conductivity. The combustion zone, which is located above the preheating zone, is constructed of highly radiating and conducting material with bigger linked pores. Combustion begins at the boundary between the two zones and spreads across the combustion zone. The experiment is conducted on four different types of porous media. In the first scenario, a set of metal balls is used as a porous burner.

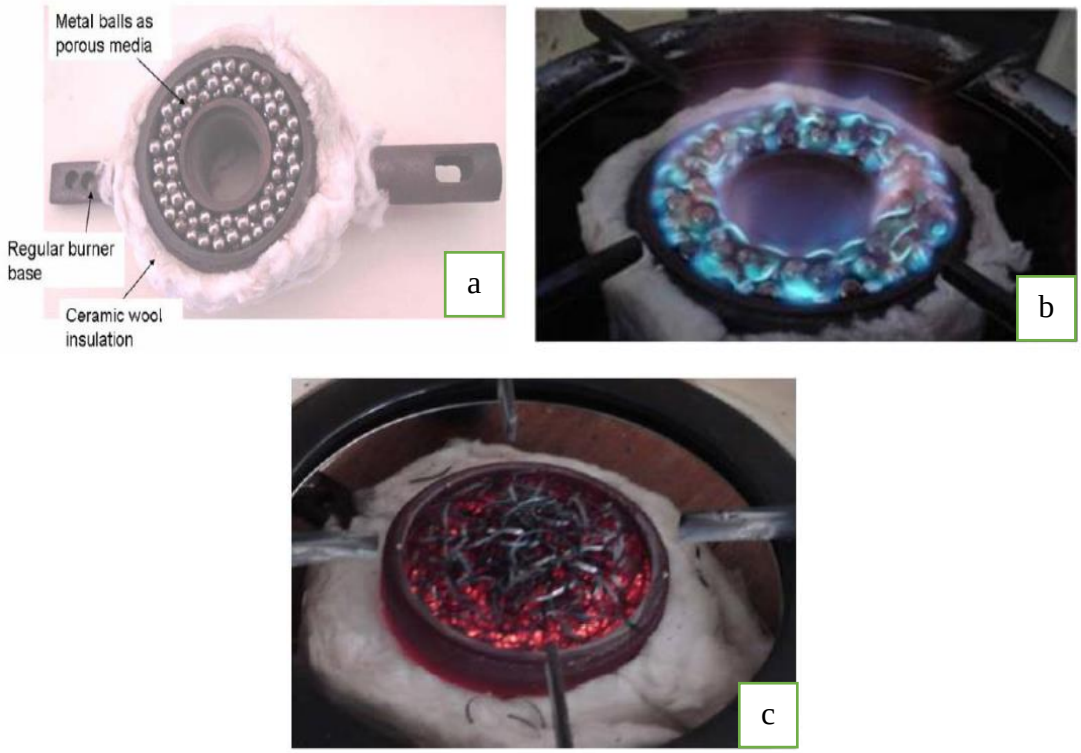

Figure 2-8 a) sealed mixing tube of a standard burner with a porous medium made of metal balls within. b) Metal ball used as porous media. C) Combustion in the porous medium of metal chips(Pantangi et al., 2007)

In the second scenario, metal balls are replaced with pebbles with dia. of 3 mm to minimize unwanted combustion in the preheating zone. Combustion was not seen in this zone due to the limited heat conductivity and emissivity of stones. In this situation, the thermal efficiency was found to be 69 percent. In the third case, ceramic wool insulation was installed along the sides

and bottom of the mixing tube to prevent loss of heat. Additionally, to reduce radiation heat loss upstream, the distance between the top surface of the mixing chamber and the bottom surface of the pan was lowered, and Thermal efficiency increased by 72 percent as a result of these changes. In the fourth case, metal balls in the mixing chamber's combustion zone were replaced with mild steel chips to create flameless combustion. As expected, the metal chip matrix, unlike metal balls, found to be red hot and had no flame.

To make the earlier experiment more reliable, Pantangi et al. (2011)examines the research on porous media burners for cooking using LPG fuel. The burner is made up of two layers of the porous medium. Silicon carbide makes up the combustion zone, whereas alumina balls make up the preheating zone. The burner's performance in the context of emission traits and thermal efficiency is examined for various equivalence ratios and thermal loads for a given burner diameter (wattages). The thermal efficiency of both the traditional LPG cooking burners and the PRB was calculated using the BIS (Bureau of Indian Standard): 4246:2002 water boiling test. The PRB for LPG cooking stoves employed in this investigation is depicted schematically in Fig. 2.9. The two-layer PRB's CZ (combustion zone) is comprised of a porous SiC (silicon carbide) matrix. PZ is prepared from a 5 mm Al_2O_3 balls. The PRB consists of a combustion zone, a preheating zone, a wire mesh to support the preheating zone, a burner casing, and a mixing tube made up of Teflon. The experiments were performed with different diameters and thicknesses of the combustion zone.

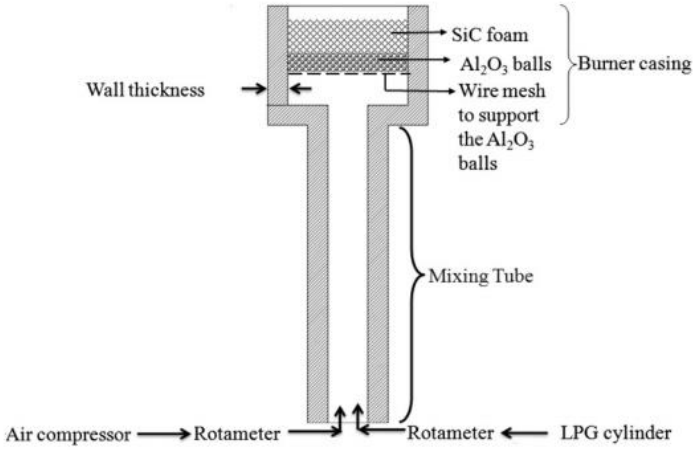

Figure 2-9 Schematics of the porous radiant burner by Pantangi et al. (2011)

The trials were carried out with various combustion zone sizes and thicknesses. The burner's diameter was expanded in 1.0 cm increments from 6.0 cm to 10.0 cm. The rotameters with control valves were used to measure the fuel and airflow rates. Through their respective rotameters, compressed air and LPG at a pressure of 3.0 kN/m^2 were delivered to the mixing

pipe. The thermal efficiency of LPG cooking stoves was measured using the water boiling test as prescribed by the Bureau of Indian Standards BIS: 4246:2002. The outcome then reveals that, at increasing wattages, reaction zone located at bottom of the burner, according to axial temperature measurement. For larger wattages, the radial temperature was found to be uniform, which is a desirable quality in any burner. The maximum η_{th} of the 8cm thickness burner was about 68%, which is 3% higher than the maximum η_{th} of the conventional LPG household cook stoves. The CO and NOX emissions of the PRBs in rang of 25-350 mg/m3 and 12-25 mg/m^3, which are much lower than the corresponding values for the conventional LPG domestic cooking stoves.

Herrera et al. (2015) uses Al_2O_3 particles from grinding waste to study stability of combustion and η_{th} in a porous media burner for LPG cooking in the food industry. mixed with SiC ceramic foam as a porous media burner. The burner is divided into two main zones: a preheating zone of 8.5 cm in height where particles of Al_2O_3 resulting from waste grinding in industrial ball mills are packed, and a second zone of 8.5 cm in height where particles of Al_2O_3 resulting from waste grinding in industrial ball mills are packed. These particles have an average equivalent diameter of 11 mm, and it is thought that using this material will lower the cost of producing a porous burner. The main combustion zone is the second burner zone, which is made up of SiC ceramic foam disks with an exterior surface area of 0.02 m^2 and a pressure of 20 ppi (pores per inch).

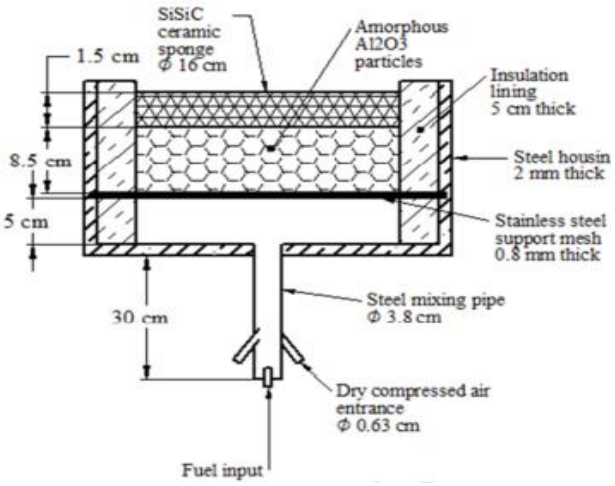

Figure 2-10 Experimental setups and Scheme of the porous burner by Herrera et al. (2015)

It is 1.5 cm tall and has a diameter of 16 cm. Both materials are surrounded by a ceramic fiber lining as material of insulation to reduce loss of heat through metallic housing of the burner. The Al_2O_3 particles are supported in a metallic mesh with a diameter of 6 mm in each opening.

Dry air is provided through a mechanical screw air compressor at 700 bar and its flow is regulated by an appropriate control needle valve. Liquefied Petroleum Gas (LPG) is delivered to the burner from a pressurized cylinder. Two methods are used to assess thermal efficiency. The thermal efficiency of the convection-radiation technique is 15.7-24 percent, which is lower than the thermal efficiency of a traditional free flame burner, due to the use of an appropriate burner diameter and a lower temperature on the ceramic foam wall. The thermal efficiency obtained with the conduction technique is 7-14 percent higher than that of a traditional free-flame LPG burner.

Pradhan et al. (2018) investigated the performance and emissions of a porous radiant burner for residential cooking with LPG as the fuel. Two types of burner shapes are used in this research. The initial shape of porous material used in the experimental setup was a circular shape with an 80mm diameter and a 65mm thickness, along with the components for creating a porous radiant burner. The second shape is rectangular, measuring 80mm in length and 65mm in height, with the same basic design as the circular one.

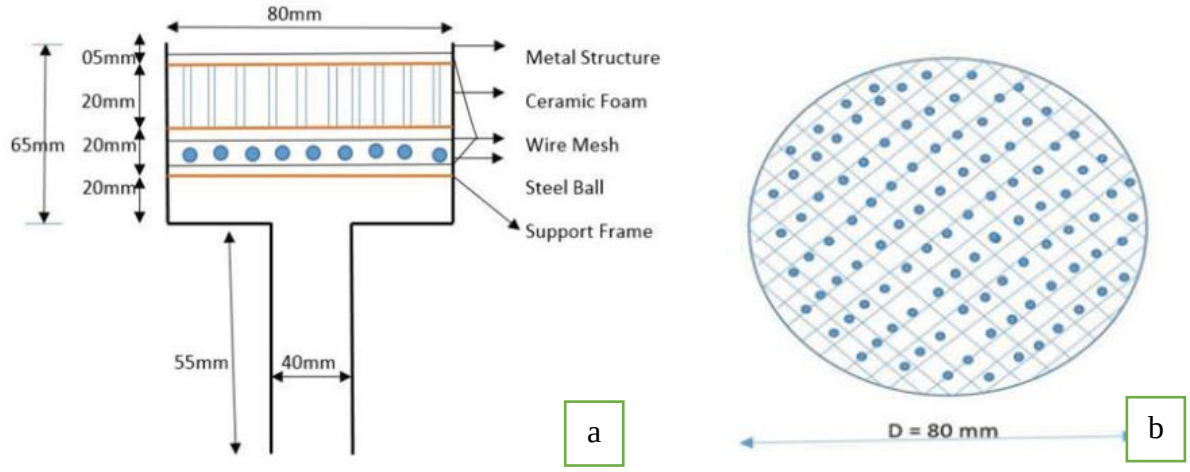

Figure 2-11 Schematic of the circular PRB with dimensions (a) Front view and (b) Top view.(Pradhan et al., 2018)

Experiments were carried out in both a controlled and open environment, according to Bureau of Indian Standards (BIS): 4246:2002 criteria, with five different fuel velocities (3.6-0.4 m/s) within the range of 1-2 kW as input parameters. The greatest temperature reached was 1247°C, according to the temperature profile result. This may be due to the dominance of both convection and radiation heat transmission in this zone. With a fringe rate of V = 2 m/s equivalent to a power input of 1.75 kW and a porosity of 85 percent, the maximum thermal efficiency of the circular porous ceramic burner (CPRB) was found to be 71.78 percent. For both CPRB and SPRB, the NOx emission levels corresponding to the optimum firing rate of 2 m/s were 29 ppm.

Although the temperature in the combustion zone is not particularly high in CPRB and SPRB, the generation of quick NOx is limited due to the short residence duration. CO emission values for CBs were similar, ranging from 1.32 to 2.28 percent and 0.7 to 0.92 percent, respectively. When compared to traditional burners, CO emissions from these CPRBs were lower due to better fuel combustion in the combustion zone.

Based on the principles of combustion of LPG fuel in PRB-assisted stoves, Devi et al. (2019) show the combustion behavior of the Porous Radiant Burner (PRB), which was developed in-house and can be used in industrial incinerators or bio-medical solid waste disposal systems. The PRB is made of double-layer porous media technology and is designed to fire at a rate of 5-10 kW. The mixing chamber, Preheat Zone (PZ), and Combustion Zone make up the burner (CZ). The CZ is a 20 mm thick Silicon Carbide (SiC) reticulated foam with a porosity of 90%, whereas the PZ is a 7 percent porosity Alumina (Al2O3) ceramic with a thickness of 15 mm. Both the CZ and the PZ are the same size (120 mm). After flowing via a Coriolis mass flow meter, biogas is directed to the burner, and compressed air is delivered to the burner via the flow meter. In the mixing chamber, the fuel and air are combined.

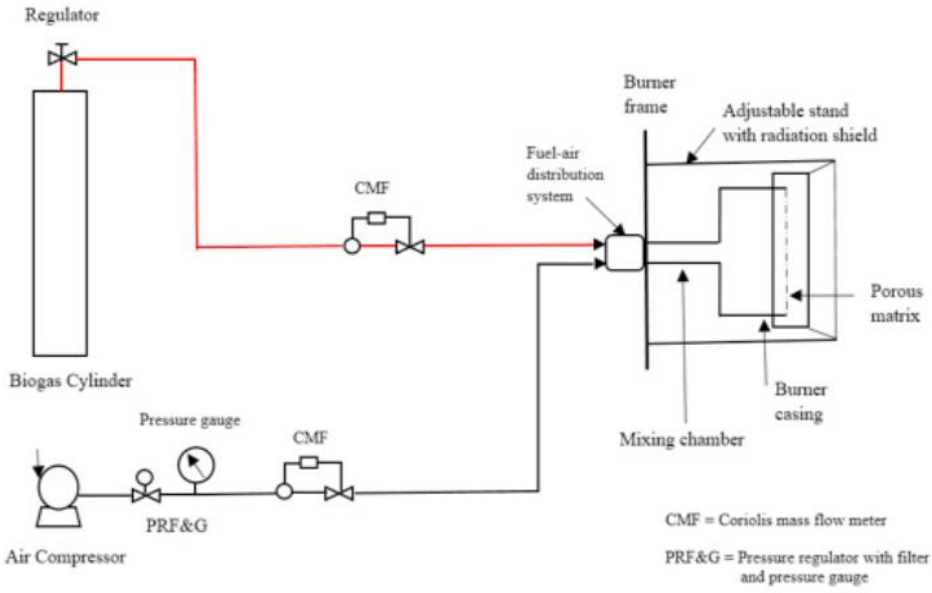

Figure 2-12 Experimental setups of biogas operated PRB by Devi et al. (2019)

PRBs have a lean burn combustion characteristic, as evidenced by the consistent working equivalence ratio range of 0.75-0.97. The maximum CO and NOx readings for PRB at 5 and 10 kW fire rates were 101 and 3 ppm; 165 and 8 ppm, respectively, indicating cleaner combustion from the in-house produced PRB. CO and NOx pollutant emissions were reduced by up to 95 percent and 85 percent, respectively.

Kaushik and Muthukumar (2019) investigate combustion characteristics and the performance of 50/50 (by volume) blending of waste vegetable oil (WVO) and kerosene in conventional kerosene pressure cook stove (CKP) and porous kerosene pressure cook stove (PKP) with input power varying from 1.5-3KW experimentally. A water boiling test and controlled cooking test were performed in the two stoves. From the results, the thermal efficiency of CKP is obtained at 28.6-36.2% and 37.8-45.3 in the case of PKP. This is due to lower operating power yields maximum efficiency and decrement in thermal efficiency in the case of CKP because increasing in convective and radiative heat loss results from increasing in power which greatly increases the flame height.

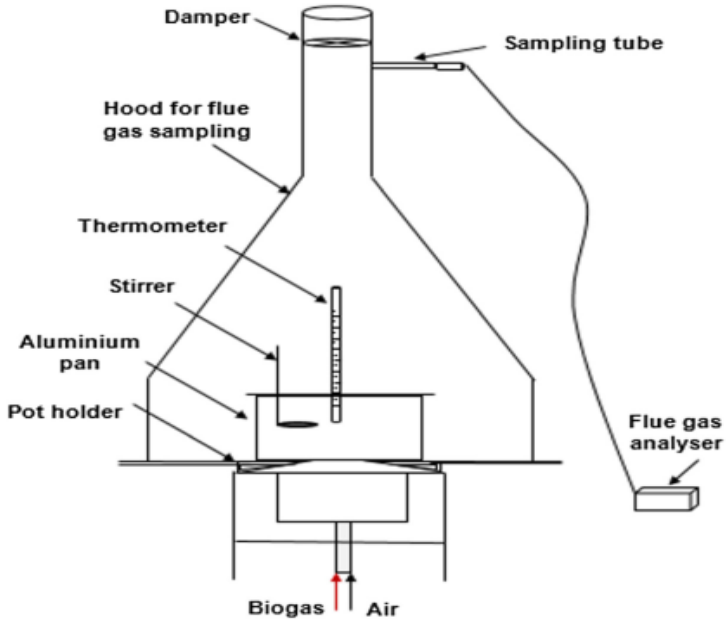

Figure 2-13 Experimental setups for thermal performance tests by Kaushik and Muthukumar (2019)

In the case of PKP, efficiency is improved due to the introduction of a highly emissive porous material resulting in the result of radiative and convective heat transfer combined together. CO and NOx emissions were 905-1300 ppm and 84-180 ppm, respectively in the case of CKP, and 361-664 ppm and 13.8-47 ppm in the case of PKP. Effective combustion and longer residence times in PKP result in lower CO emission than CKP, whereas lower surface temperature in PKP results in reduced NOx emission. Due to combustion in porous media, PKP shows improved performance and exhibits energy saving, less emission, and lower overall cost.

Kaushik et al. (2021) analyzes biogas combustion properties in a Porous Radiant Burner (PRBBG) built for residential cooking equipment in another study. The developed PRB is made of silicon carbide and alumina matrices with a 90 mm combustion and preheat zone. The

enclosure is built of casted cement that can withstand high temperatures. The biogas is compressed and stored in the balloon.

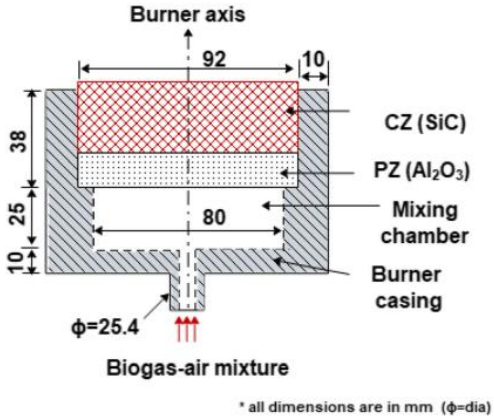

Figure 2-14 Schematic of PRB for Biogas (Kaushik et al., 2021)

In this work, three performance indicators are used to characterize the performance of the burner. These are stability, thermal efficiency, and emission. In PRB, the biogas-air combination is sprayed into the top surface of SiC after entering via the Al2O3 porous matrix.

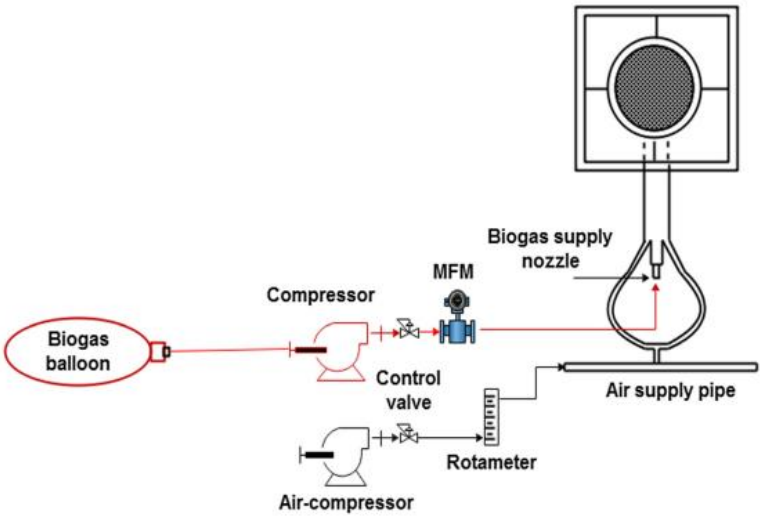

Figure 2-15 Schematic diagram of the experimental setup (Kaushik et al., 2021)

According to the results of the experiments, a uniform temperature distribution throughout the burner surface improves combustion performance. CO and NOx concentrations in PRBBG are lower than 80 ppm and 4 ppm (at 3% O_2), respectively, and are comparable to conventional burners. PRBBG achieves a maximum 18 percent improvement and 73 percent and 80 percent reductions in CO and NOx as compared to its traditional counterpart. The PRBBG's overall performance suggests that it could be a viable alternative to biogas cook stoves.

2.9 Literature Summary

Table 3 Summary of related literature works

No.	Title	Findings	Reference
On Biogas Stove With Conventional Burners			
1	Design, Optimization, and CFD Simulation of Improved Biogas Burner for 'Injera' Baking in Ethiopia	Improved biogas injera baking stove, reduction of traditional inefficient biomass burning, the optimum burner manifold diameter is 26 cm with uniformity of heat distribution throughout the baking pan	(Mulugeta et al., 2017)
2	Design of Biogas Stove for INJERA Baking Application	The designed burner has acceptable fuel consumption and equivalent time for baking with biomass stoves, burner has a fuel consumption rating of 0.93 m^3/hr, and has an insulation material prepared from different materials which have a good insulation properties for community-level baking	(Kebede & Kiflu, 2014)
3	Design, Fabrication, and Testing of Biogas Stove for 'Areke' Distillation: The Case of Arsi Negele, Ethiopia, Targeting Reduction of Fuel-Wood Dependence	Efficient, lower emission with economically feasible, 54.8 & 43.6% at the higher flame intensity and relatively lower flame intensity, biomass fuel dependency reduced by 27.7% by reducing 32, 763.70 tons of GHGs emission annually	(Demissie et al., 2016)
4	Theoretical and Experimental Performance Analysis of a Novel Domestic Biogas Burner	developed burner has an improved thermal efficiency of 67.01%, the fuel consumption of the developed burner was 736 g/L which is lower as compared to other burners manufactured locally	(Petro et al., 2020)
	On CFD Simulation of Porous Radiant Burners		
5	Computational fluid dynamics modeling of porous burners	A numerical approach will be used to improve the design of porous burners for ultra-lean combustion, similar temperature profile, and higher adiabatic flame temperature due to heat recirculation of solid porous matrix	(Tierney et al., 2009)

6	CFD Analysis of Porous Medium Burner for Domestic Cooking Application	Obtaining max surface temperature of 2246 K at burner model having center pipe length and diameter of 27.5 and 25 mm, and at higher temp flame starts at PZ' flashback increases as center pipe length increases				(Soma et al., 2018)
7	Numerical Simulation of a New Porous Medium Burner with Two Sections and Double Decks	Inner temp. peak value reaches 2700 K at an equivalence ratio of 0.85 and flow velocity of 0.85m/s, reducing the concentration of major pollutants such as NOx which is lower than standards				(Jia et al., 2018)
8	Internal flow analysis of a porous burner via CFD	Very low-pressure drop throughout means low pumping power requirement, safe functioning, and avoiding self-ignition.				(Abdulkarim et al., 2019)
	On Experimental Analysis of LPG and Biogas Stove With PRB					
		Qualitative	**Quantitative**			
			Efficiency	**CO**	**NOx**	
9	A proposed porous radiant recirculated burner (PRRB)'s parametric thermal efficiency studies: A burner design idea	Effective energy conversion from gas enthalpy to thermal radiation	η_{th}= 79% with PRRB 65% with PRB and 56% with CB	At 2.5 Kw 2980 ppm for SB, 3000-3500 ppm for PRB	4-22 PRB, 22-102 CB, >177 ppm with PRRB	(Jugjai & Sanitjai, 2007)
10	Performance Evaluation of Porous Media Domestic LPG Cooking Stoves	Increased efficiency with the lowest CO2 and CO emission and cost saving	η_{th} =68-72% with metal balls as PZ & CZ and 73% with metal balls as PZ and chips as CZ	188 and 117 ppm	CO_2 % by volume 0.7-0.8 and 0.93	(Pantangi et al., 2007)
11	Studies on porous radiant burners for LPG (liquefied petroleum gas) cooking applications	Increased efficiency with reduced pollutant emission and less fuel consumption	increased to 68% w/c is 3% higher than CB	50-350mg/m^3 Lower than CB	NOX varies in the range of 10.0-25.0 mg/m^3,	(Pantangi et al., 2011)
12	Combustion stability and thermal efficiency in a porous media burner for LPG cooking in the food industry using	Efficient and less fuel consumption device for household application	Conv-Rad efficiency 15-25% Lower than CB Conduction Eff. 7-14% > CB	CO< 25 PPm	Undefined!	(Herrera et al., 2015)

	Al_2O_3 particles coming from grinding wastes					
13	Performance and Emission Analysis of a Novel Porous Radiant Burner for Domestic Cooking Application	Increased efficiency with the lowest CO and NOx emissions	η_{th} = 72% and 71% with CPRB and SPRB 8% than CB with a firing rate of V=2m/s	12-45ppm	12-42 PPm	(Pradhan et al., 2018)
14	Low emission biogas combustion in a porous radiant burner	Lower NOx values than CB, increased η_{comb}	η_{comb}=99.98% which is 1.76% higher than CB	5 and 10 kW 101 and 165ppm	for 5 and 10 kW, 3 ppm; and 8 ppm	(Devi et al., 2019)
15	An evaluation of the efficiency of a porous radiant cook stove powered by kerosene and waste vegetable oil (WVO)	PKP burner becomes efficient and less cooking time with reduced fuel consumption and reduced emission than CKP	37.5-45.3% for PKP, 28.6-36.2% for CKP	905-1300 ppm for CKP, 361-664 ppm for PKP	84-180 ppm for CKP, 13.8-44 ppm for PKP	(Kaushik & Muthukumar, 2019)
16	Analysis of the performance of a biogas-powered porous radiant burner for use in residential cooking	the well-distributed temperature profile was achieved, leaner biogas combustion is possible	η_{th} varies from 62-54% for ϕ=0.75-0.95	29–80 ppm	1–4 ppm lower than CB	(Kaushik et al., 2021)

2.10 Literature Closure

Porous media combustion technology is an age-old combustion method that offers numerous benefits. Materials' importance in terms of efficiency and emission has been emphasized. Over the last decade, PRB has made significant progress in both residential and commercial culinary applications. The performance of porous radiant burners has been proven, as well as their potential to replace commercial burners based on free flame combustion. Biogas has the potential to be a viable cooking option, but it requires efficient cook stoves. Furthermore, conventional biogas burners are working on the principle of free flame combustion that has unfavorable characteristics such as low limits of flammability, lower power density, higher toxic emission, and lower thermal efficiency. According to the above-mentioned works, several studies have been conducted on the utilization of porous media combustion in LPG and Biogas stoves using compressed air and compressed biogas. However, these researches, which are performed on biogas areas, are working with compressed air, which needs an additional compressor to achieve higher reactant velocity and to reduce pressure drop caused by the porosity of the porous inert burner. From the literature survey, it is also revealed that in spite of the negative impact of these additional components on the total cost and portability of the PRB cook stoves, no studies have been performed regarding developing self-aspirated PRB domestic biogas cook stove. Thus towards addressing this issue, this thesis is aims to perform both numerical and experimental analysis in developing self-aspirated PRB domestic biogas cook stove with a two layer porous media.

CHAPTER 3
MATERIALS AND METHODS

This section describes the process of selecting materials and characterizing ceramic foams, as well as the approach used to design and analyze porous radiant burner-assisted domestic cook stoves. Here it presents methods of geometric analysis of porous radiant burner and proposes an approach of selecting patterned porous media (PM) with flow characteristics similar to those of the foam. This section also describes the methodology of the experiment and the nature of the tests that will performed.

3.1 Basic Parameters in the Design of PRB

3.1.1 Combustion Fundamentals

From the basic principle of combustion expressed in El-Mahallawy and Habik (2002), combustion is a chemical reaction between a fuel and an oxidizer, which normally generates heat and light in the form of a flame. Flames can be divided into two types: premixed flames and diffusion (non-premixed) flames. Premixed flames are formed by mixing fuel and oxidizer before entering the combustion zone, whereas diffusion flames are formed by diffusion at the border between fuel and oxidizer, such that mixing and combustion occur simultaneously. In this research paper, only premixed combustion is examined. An important characteristic that defines mixture composition is the equivalence ratio (ϕ). This ratio indicates whether combustion occurs for the fuel-lean (ϕ< 1), stoichiometric (ϕ = 1), or fuel-rich (ϕ> 1) mixtures and is represented by:

$$\phi = \frac{(A/F)Stoic}{(A/F)} \qquad (3\text{-}1)$$

Where A/F= $m_{air}/m_{fuel}$is the air-fuel ratio.

Another essential feature is laminar flame speed (S_L), which defines the speed of chemical reaction between reactants and is equal to the unburned reactants' velocity (V) at stationary conditions.

3.1.2 Basic porous foam burner

As here mentioned earlier in the literature review section, conventional gas burners (CGB) directly burn the incoming mixture by producing free open flames and releasing heat through a chemical reaction between fuel and oxidizer. PMB can be considered a modified CGB with an intermediary material allowing for the passage of the gas mixture and providing heat recirculation between the post- and pre-flame zones. The distinction between PMs is often made based on pore size, which

is defined by the number of “pores per inch” (PPI) or “pores per centimeter” (PPC). The bigger the PPI/PPC value, the smaller the pores that allow for the passage of the mixture, resulting in a greater flow restriction (Samoilenko, 2018).

Flashback zone is defined as inlet velocities lower than SL, such that a flame cannot be sustained and the flame front begins to propagate into the upstream section. A quenching distance exists for flames that are defined as the critical passageway below which flame cannot propagate. For safety reasons, flashback arresting devices with openings, are smaller than quenching distance but still allow for the passage of the mixture, should be employed.

The lifting flame zone is attributed to inlet velocities that are too high in comparison with SL, and that causes the flame to be displaced downstream too far from the burner’s edge. Further increases in V results in blowing off the flame. Combustion in PM results in higher flame speeds and inlet velocities. During the design and fabrication of PRB assisted stoves, it is necessary to consider these two factors.

3.1.3 The durability of porous materials

The main materials used in PMB for flame support and heat recirculation are ceramic foams. Due to their high-temperature operation limits (Ttop> 1400 ℃) and high thermal conductivity. However, ceramics are brittle materials by nature and prone to crack formation when exposed to high-temperature gradients and thermal shocks (Samoilenko, 2018).

3.2 Description and Specification of Burner

The schematic diagram of the self-aspirated PRB for domestic cooking stoves used in the present study is shown in Figure 3-1 and the main feature of the burner except the modifications of orifice and slots were designed by Kaushik et al. (2021). Through the pressure regulator of the compressor (1), the biogas is supplied to an orifice (2). For the air entrainment, a steel-made mixing tube (4) with two slots (3) facing each side is made and the mixture of fuel and air will go through the burner port (5). The burner casing (8) of cement is made of two parts, which are the lower part with 75 mm and the upper section having 80 mm of diameter. Up to the height of the 20 mm burner casing the mixing tube (4) will be inserted. The preheating zone (6) made of cast iron is fixed at the upper section of the burner casing and the combustion zone (CZ) (8) made of SiC (silicon carbide) porous matrix placed over the preheating zone.

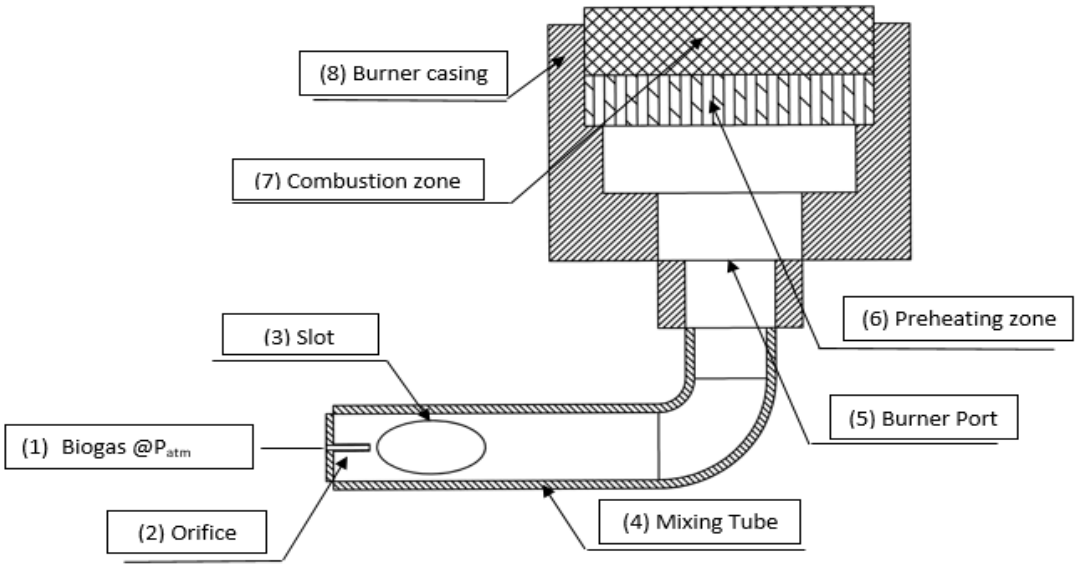

Figure 3-1 Schematic diagram of newly developed Self-aspirated PRB cook stove

The specification of the components of the self-aspirated burner, which is described in detail in the above section, is shown in the table below.

Table 4 Specifications and nomenclatures of different models of porous radiant burners.

Specification (In mm)	**Dimensions (mm)**
Burner casing inside diameter (mm)	80
Burner casing total height (mm)	70
Mixing tube inside diameter (mm)	20
Mixing tube length (mm)	100
The thickness of CZ (SiC, P=90%) (mm)	20
The thickness of PZ (cast iron, P=20%) (mm)	10

The numerical simulation will be performed with different burners. For the newly developed self-aspirated PRB domestic biogas stove, the orifice and slot dimensions have to be determined for the replacement of the forced air supply system in the existing PRB stoves to achieve a lower pressure drop and increased fuel-air mixture velocity. Three different types of orifice diameter, slot height, and length are prepared for the numerical investigation and the orifice and slot dimensions that have better results will be fabricated and used in the experimental investigation. The dimensions of the orifice and slots in this investigation are given in Table 5.

Table 5 Specifications and dimensions of orifice and slots

S.N	Case	Orifice diameter (mm)	Port height (mm)	Port length (mm)
1	1	0.8	10	15
2	2	1	15	20
3	3	1.2	20	25

3.3 Selection of materials for porous media combustion

Cast iron and silicon carbide (SiC) are selected as suitable materials for this burner application. Cast iron was recognized as a high-temperature-resistant material. Silicon carbide (SiC) shows good thermal shock resistance, mechanical strength, and conductive heat transport. SiC also has a high melting point (3260 K), against cyclic thermal stress and strength retention at the peak regenerator temperature (1673 K), and excellent oxidation resistance. Metallic materials were found less suitable for PMC because of their inadequate thermal stability and high thermal. Iron-Chromium–Aluminum-alloys and nickel-base alloys were found suitable for some applications but they were said to be comparatively less heat resistant. Structures of ceramic foams with different base materials were observed to possess high porosity, good conduction heat transport, low thermal inertia, low radiation heat transport properties, and relatively high-pressure drop. The effective thermal conductivity of an anisotropic porous composite medium could vary largely with the component fractions(Harris, 1995), (Huang et al., 2011).

Table 6 Mechanical and thermal properties of SiC and Cast iron

Parameters	Values	
	SiC	Cast Iron
Density, (g/m^3)	3.3	7.1
Maximum operational temperature, $T_{max, op}$ (°C)	1400	1355
Thermal conductivity (20°C), k (W/(mK))	110	70
Thermal conductivity (1000°C), k (W/(mK))	42	20
Thermal expansion coefficient, α_t (μm/(mK))	4.8	11
Tensile strength, σ_t (MPa)	240	1450
Young's Modulus, E (GPa)	270	655
Poisson's Ratio, υ	0.35	0.37
Thermal shock resistance parameter, R (K)	150	-

3.4 Methodology

The general methodology of this research paper starts with data collection from various organization and literature review from previous papers on the design of PRB and conventional burners, biogas digesters, and cook stoves. Method of design of PRB will go through modeling and CFD simulation of the existing forced air supply (base line) and newly proposed self aspirated PRB cook stove in ANSYS fluent. The results from the CFD analysis will be conducted and the optimum design of a new self-aspirated PRB that have a better performance than the other proposed models will be selected and fabricated. Then the experimental performance analysis will be done on the fabricated self-aspirated PRB biogas stove and will compared with the existing conventional burner biogas stove. The overall work plan for this thesis is listed in the following methodology flowchart.

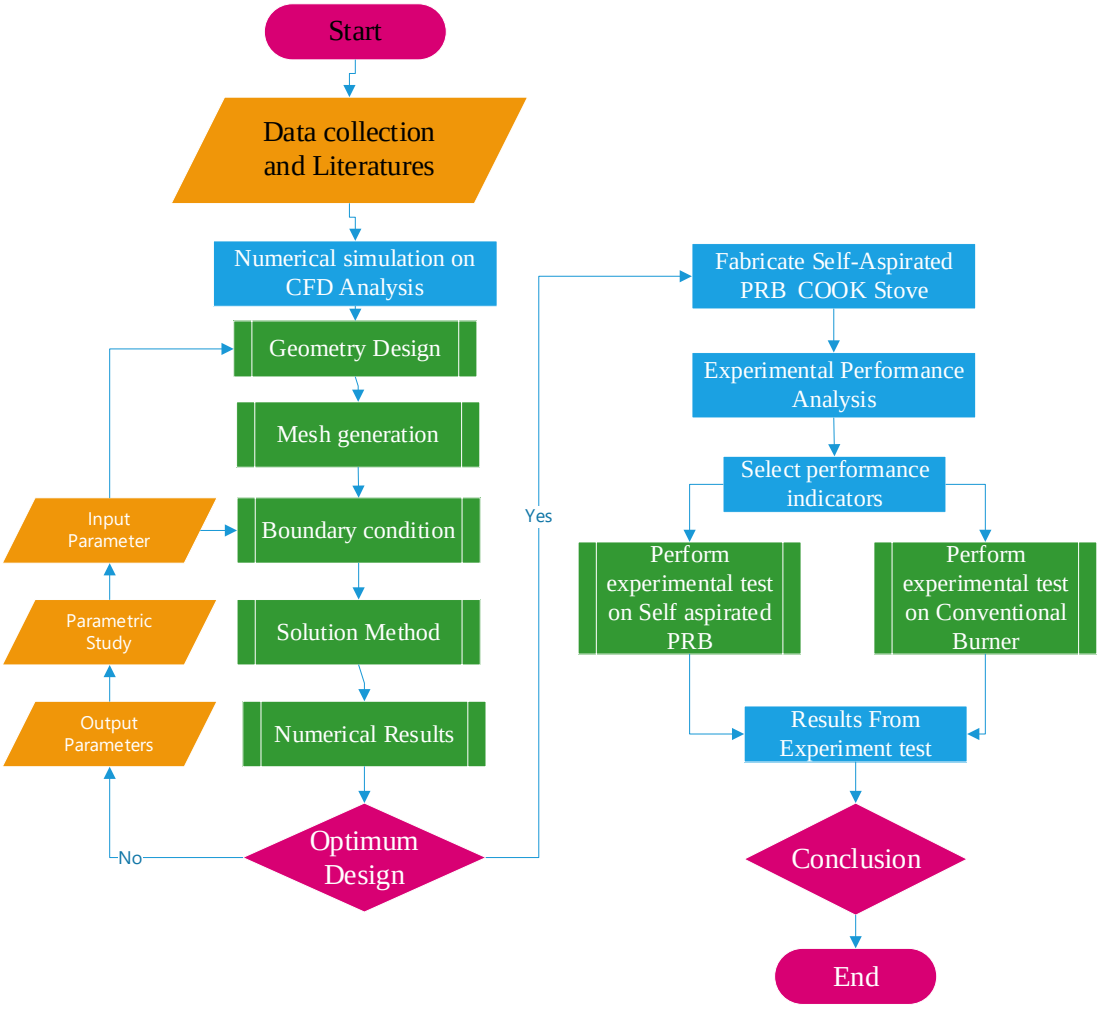

Figure 3-2 Flow chart of the methodology

3.5 Numerical Modelling

The presence of both solid and fluid (gas or liquid) media characterize porous media combustion (PMC), which is described by Mujeebu et al. (2010), and governing equations must be developed for both phases. In this numerical modeling section, Porous Medium (PM) is assumed to emit, absorb, and scatter radiant energy. The performance of the burner is examined in relation to the optical depth, solid heat conductivity, dispersion albedo, upstream environment reflectivity, and interphase heat transfer coupling. In addition, low solid thermal conductivity, low scattering albedo, and high inlet environment reflectivity produced a high radiant efficiency. The system consisted of a packed bed or foams in which a CH_4–air mixture combusts inside it. Radiative heat transfer in the packed bed or foams is modeled as a diffusion process, and the flow and temperature distribution in the packed bed or foams will be determined. Finally, the numerical results will be compared with available experimental and simulation data for a similar system.

3.5.1 One Dimensional Modelling

3.5.1.1 Governing Equations

From the literature on numerical modeling in PMC by Ziabasharhagh and Mohammadi (2012), modeling governing equations of porous media is followed by these general assumptions. The thermos-physical properties of the air such as density, thermal conductivity, and specific heat are assumed to be functions of the temperature. Usually, the pressure drop through the porous burner is not that high (with high porosity of PM) and its effect on the thermos-physical properties can be neglected. In general, the properties of the solid phase may be assumed to be constant, and assumed that there is thermal non-equilibrium between the gas and solid phases. The air and fuel are completely premixed at a given temperature and equivalence ratio. Flow is incompressible and one-dimensional so the momentum equation need not be solved explicitly. The governing equations are the same as those listed in Ziabasharhagh and Mohammadi (2012). Therefore, there are two energy equations to model the energy transport in the system. The basic equations governing the combustion of gaseous fuels in PM and the resulting heat transfer modes are energy, continuity, momentum, and species conservation equations. In addition, the mathematical models of chemical reaction kinetics and radiation effects of solid and gas phases are also included.

Continuity equation

$$\frac{\partial}{\partial t}\left(\rho_g \varepsilon\right)+\frac{\partial}{\partial x}\left(\rho_g u \varepsilon\right)=0 \tag{3-2}$$

Gas-phase energy equation

$$\rho_g c_g \varepsilon \frac{\partial T_g}{\partial t}+\rho_g c_g \varepsilon u \frac{\partial T_g}{\partial x}+\sum_i \rho_g \varepsilon Y_i V_i C_{gi} \frac{\partial T_g}{\partial x}+\varepsilon \sum_i \omega_i h_i w_i=\varepsilon \frac{\partial}{\partial x}\left[\left(k_g+\rho_g c_g D_{II}{}^{D}\right)\frac{\partial T_g}{\partial x}\right]-h_v\left(T_g-T_s\right) \tag{3-3}$$

Solid phase energy equation;

$$\rho_s c_s\left(1-\varepsilon\right)\frac{\partial T_s}{\partial t}=k_s\left(1-\varepsilon\right)\frac{\partial^2 T_s}{\partial x^2}+h_v\left(T_g-T_s\right)-\frac{dq_r}{dx}=0 \tag{3-4}$$

Species transport equation;

$$\rho_g \varepsilon \frac{\partial Y_i}{\partial t}+\rho_g \varepsilon u \frac{\partial Y_i}{\partial x}+\frac{\partial}{\partial x}(\rho_g \varepsilon Y_i V_i)-\varepsilon \dot{\omega}_i W_i=0 \tag{3-5}$$

Where $V_i=-(D+D_{in}{}^{d})\frac{1}{X_i}\frac{\partial X_i}{\partial x}$

Density;

$$\rho=\text{Constant density}$$

Radiation;

$$q_r(x)=-\frac{16}{3}\frac{\sigma T_s^{\,3}}{\beta}\frac{dT_s}{dx} \tag{3-6}$$

3.5.1.2 Boundary Conditions

The following boundary conditions are considered in the computations:

Inlet	$T_g=T_{f,inlet}$	$\frac{\partial T_s}{\partial x}=0$	$\frac{\partial T_s}{\partial x}=0$
Outlet	$\frac{\partial T_g}{\partial x}=0$	$\frac{\partial T_s}{\partial x}=0$	$\frac{\partial Y_i}{\partial x}=0$

3.5.1.3 Solution Method

The time integration is performed using a combination of implicit finite difference and finite volume method on a uniform-adaptive or non-uniform mesh. The convective terms are up winded

and a second-order method is used to discretize the diffusive terms. The initial condition was also given to the system of discretized equations.

3.5.2 Two Dimensional Modelling

In the two-dimensional model, a comparison is made between the local thermal equilibrium and thermal non-equilibrium approaches by different researchers. The volume-averaged treatments are unable to predict the pore-level, local high-temperature region in the gas phase, and the pore-level variation in the flame speed concerning the flame location in the pore. The gas and the solid phases consider in non-local thermal equilibrium, and separate energy equations use for the two phases. While the gas phase was thought to be transparent to radiation, the solid phase can be presumed to absorb, emit, and scatter radiation. The transient two-dimensional energy equations can be resolved using the alternating direction implicit (ADI) scheme. Methane–air combustion with one-step, multi-step, and detailed chemical kinetics are used to model the combustion, like one-dimensional combustion modeling. From the straightforward Rossel method to the intricate discrete ordinate method, the radiative portion of the energy equation can be modeled. Air moves axially through a constant area duct filled with a porous layer of thickness L in the flat plate burner. The air flows radially through an annular porous matrix in the cylindrical and spherical burners.

3.5.2.1 Two-dimensional Governing Equations

Energy in the gas phase equation is given as follows;

$$\frac{\partial}{\partial t}\left(\varphi\rho_g c_{pg} T_g\right)+\frac{1}{r^n}\frac{\partial}{\partial r}\left(\varphi\rho_g c_{pg} r^n \upsilon T_g\right)=\frac{1}{r^n}\frac{\partial}{\partial r}\left(\varphi k_g r^n \frac{\partial T_g}{\partial r}\right)-\left(1-\varphi\right)h_v\left(T_g-T_s\right)+\varphi\Delta H_c S_{fg} \qquad (3\text{-}7)$$

Where φ, ρ_g, r, C_{pg}, T_g, v, k_g, h_v, H_c and S_{fg} are the porosity, density, radial position, specific heat, temperature, velocity, thermal conductivity, volumetric heat transfer coefficient, enthalpy of combustion and rate of fuel consumption per unit volume, respectively. Subscripts *g* and *s* refer to gaseous and solid phases.

The energy equation for the solid phase;

$$\frac{\partial}{\partial t}\left(\rho_s c_s T_s\right)+\frac{1}{r^n}\frac{\partial}{\partial r}\left(r^n k_s \frac{\partial T_s}{\partial r}\right)-h_v\left(T_s-T_g\right)-\nabla\bullet F \qquad (3\text{-}8)$$

The term *F* represents the radiative transport equation and is given by:

$$\nabla\bullet F=-\left(1-\omega\right)\left(G-4E_b\right) \qquad (3\text{-}9)$$

Where ω is the single scattering albedo and the irradiance G is governed by;

$$\nabla^2 G = \eta^2 \left(G - 4E_b \right) \tag{3-10}$$

$$\eta^2 = 3\beta^2 \left(1-\omega\right)\left(1-g\omega\right) \tag{3-11}$$

Where E_b is the Planck black body emitted flux and G is the radiative flux.

The conservation equation for the mass fraction of the fuel is given as follows:

$$\frac{\partial}{\partial t}\left(\rho_g m_f\right) + \frac{1}{r^n}\frac{\partial}{\partial r}\left(\rho_g r^n v m_f\right) = \frac{1}{r^n}\frac{\partial}{\partial r}\left(r^n D_{AB}\rho_g \frac{\partial m_f}{\partial r}\right) - S_{fg} \tag{3-12}$$

Where m_f is the fuel mass fraction and D_{AB} is the diffusion coefficient. The n value is set to 0, 1 and 2 for spherical, radial, and axial flow burners, respectively.

A single-step Arrhenius-type chemical kinetic equation as given below is normally adopted in modeling the combustion:

$$S_{fg} = f \rho_g{}^2 m_f m_{o_2} \exp\left(-\frac{E}{RT_g}\right) \tag{3-13}$$

Where f, m_{O2}, E, and R refer to pre-exponential factor, oxygen mass fraction, activation energy, and gas constant, respectively.

3.5.2.2 Boundary conditions for two-dimensional modeling

The following boundary conditions are adopted for the gas, solid, and species:

Gas;

$$T_{g|r=r_{in}} = 0 \text{ at } r = r_{in}$$

$$\frac{\partial T_g}{\partial r}\Big| r = r_{out} = T_{in} \text{ at } r = r_{out}$$

Solid;

$$h_{in}\left[\left(T_{g,in} - T_{s|r=r_{in}}\right)\right] + \sigma E_{in}\left[\left(T^2{}_{in,anb} - T_s^4\Big|_{s|r=r_{in}}\right)\right] = -k_s \frac{\partial T_s}{\partial r}\Big|_{r=r_{in}} \text{ at } r = r_{in}$$

$$h_{out}\left[\left(T_{out,in} - T_{s|r=r_{out}}\right)\right] + \sigma E_{out}\left[\left(T^2{}_{out,anb} - T_s^4\Big|_{s|r=r_{out}}\right)\right] = -k_s \frac{\partial T_s}{\partial r}\Big|_{r=r_{out}} \text{ at } r = r_{out}$$

Species:

$$m_f = m_{f,in} \text{ at } r = r_{in}$$

$$\frac{\partial m_f}{\partial r} = 0 \text{ at } r = r_{out}$$

3.5.2.3 Two-dimensional solution procedure

The control volume approach, or the finite-difference method, can be used to solve the governing equations. The solution is advanced in time by using a fully implicit technique and this was necessary due to the stiffness of the governing matrix of the problem. Also, it is necessary to use an adaptive grid, or a very fine grid, to insure the accuracy of the solution. The based code can be solved using alternative direction implicit (ADI) finite volume formulation. The pressure field is solved using the SIMPLE method in steady state and PISO intransient state. The gridding system should prove to be sufficient by testing several grids' sizes.

3.6 Numerical Simulation of PRB in CFD

CFD is a virtual prototyping tool that guides to build of precision flow models by solving different transport equations. The combustion flow features can be analyzed in detail with CFD. Temperature, mixing of different species, flow velocity, concentration and flame stability, and concentration of combustion species can be computed for different types of model geometries with a high level of accuracy. The chemical and physical phenomena of the reacting flow may be simulated by solving a generalized set of conservation equations numerically, which includes the equation for conservation of mass, momentum (Navier Stokes equations), and energy. Additional equations are required for modeling turbulence and combustion. The fundamental approach for numerical simulation of the governing equations is the finite element or finite difference approximations.

The basic steps to perform CFD analysis:

1. **Pre-processing,**

- ❖ CAD Modeling -The creation of CAD models using CAD modeling tools to create the geometry of a part/assembly that we want to perform FEA. CAD models may be 2D or 3D.
- ❖ Meshing- Meshing is an important operation in the CFD. In this operation, the CAD geometry is discretized to a large number of small Elements and nodes. The setting of nodes and elements in space in an appropriate manner so-called mesh. Accuracy analysis and duration depend on the mesh size and orientation. With the increase in mesh size CFD analysis speed decreased but increased accuracy.

- ❖ Boundary Conditions- Determining the desired boundary conditions for the problem of speed, mass flow rate, temperature, heat flux, etc.

2. **Solution**

- ❖ Methods of the solution- Choosing a solution method to solve the problem that the first-order, second order
- ❖ Solution Initialization: initialized solution to obtain an initial solution to the problem. Post Processing- To view and interpretation of results. The result can be viewed in various formats: chart, values, animation, etc.

3. **Results or Post-processing data**

For the computational approach, designing the model and grid generation and executing the required physics for modeling have been carried out by ANSYS 2021 R2 CFD environment. The burner studied in this model includes mainly four components, which are the Burner casing, mixing tube, Combustion zone, and preheating zone. Four different burner model geometries, namely CZ and PZ with three different orifice diameters have been considered to investigate the performance of the burner.

3.6.1 Geometry Design

Figure 3.3 is the schematic diagram of the burner system comprised of the burner Casing, mixing tube, combustion zone, and preheating zone. The original mixing tube has a length of 10 cm with an external diameter of 2.5 cm as well as 2 mm of thickness. The material is stainless steel with a straight inlet and outlet shape. The burner casing has 7 cm long and in this investigation, two different zones of the same diameters (80mm) have been considered. As discussed in section 3.2 the self-aspirated and forced air supply type burners are presented in Figure. Both burners have preheating and combustion zones with thickness of 10 mm and 20mm made from cast iron and silicon carbide. The PRB on the left side is the one, which uses both the compressed air and compressed biogas for higher velocity of reactant and lean combustion of biogas, and the PRB on the right side is a self-aspirated PRB, which uses compressed biogas and naturally draft air for higher reactant velocity and lean combustion of biogas.

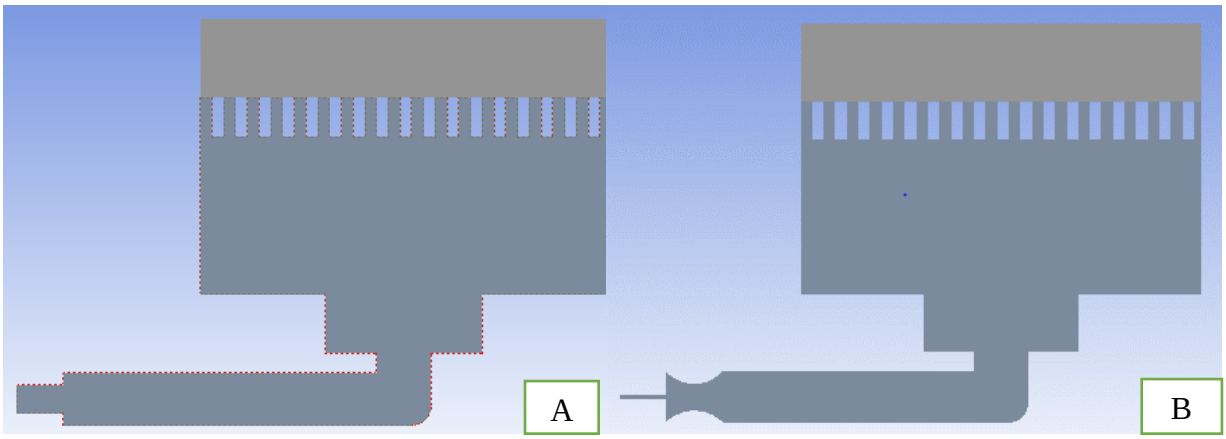

Figure 3-3 2D Geometry of (a) forced air supply and (b) self-aspirated PRB

3.6.2 Grid Generation

Creating an appropriate and precise mesh is one of the most crucial tasks in finite element analysis since it helps to reduce error and brings the solution considerably closer to the target value. This research needed to create a precise and suitable grid that took into consideration the high-speed gas injection velocity, air entrainment from the injection, turbulent mixing, wall thickness, and flame growth at the top of the burner. To create a finer mesh, Ansys's mesh generation environment allows the user to appropriately define parameters such as the maximum element size, minimum element size, maximum element growth rate, curvature factor, and resolution of the narrow region. Among these, maximum element size restricts the size of an element that is permitted, whereas minimum element size specifies the smallest size that an element is permitted to have. The maximum element growth rate sets the maximum rate at which the size of an element can increase from a region with small elements to a region with larger elements, and the curvature factor sets the ratio between the size of a boundary element and the curvature radius to establish the size of a boundary element concerning the curvature of a geometric boundary. The default grid will be generated on the ANSYS user interface and the grid size will becomes more finer for a better results. And the dependency of the results on the grid size will be tested on a selected model and the result will plotted on the first section of the next chapter. The simulation of remaining models will be performed under the finer grid size which is determined in the grid independence test.

3.6.3 Selection of suitable physics, boundary conditions, and solver

To conduct the computational investigation, acceptable physics has to be chosen after constructing the 2D geometry and setting up the proper grid. The mixing process in the tube and the flow have

both been treated as turbulent in this manner. The features include Turbulent Flow k-, Transport of Concentrated Species, Heat Transfer in Fluids, Reacting Flow, and Non-isothermal Flow due to the existence and reactivity of chemical species and taking into account both isothermal and non-isothermal states. It is crucial to select the precise boundary conditions, together with any other essential regulating elements and parameters, for each physics. The Turbulent Flow k-ω, which is used to simulate single-phase flows at high Reynolds numbers, must be chosen as the first physics. For weakly compressible flows, incompressible flows, and compressible flows at low Mach numbers, the physics interface is appropriate (less than 0.3). The Reynolds-averaged Navier-Stokes (RANS) equations for momentum conservation and the continuity equation for mass conservation are the equations that are resolved by the Turbulent Flow, k-ω interface.

Methane-air reaction with a volumetric approach should be selected when the species transport mode is turned on in the model section of Ansys Fluent, however, premixed combustion should be chosen in the case of PRB. No slip is the default boundary condition to model solid walls for the wall. The fluid velocity concerning the wall velocity is zero in a no-slip wall. That implies that u = 0 for an immovable wall. For the porous section, the porosity of 0.9 will be assigned for CZ and the 0.2 for PZ. Both forced air supply (base line) and self-aspirated PRB will operate at the same atmospheric conditions. The injector entry has been selected as the inlet as a fully developed flow, where the average velocity is set from experimentally utilized various volume flow rates in Standard Liters per Minute (SLPM). Additionally, the simulation's input values are presented in Appendix I mixing simulation background calculations section. Hybrid initialization will be used to start the simulation, and a CFD calculation will be performed after 2000 iterations. The findings of the computational fluid dynamic study will be given in the following chapter.

3.7 Experimental Analysis

3.7.1 Experimental Setup

Challenges emerge when conducting a validation experiment with biogas from an anaerobic digester. Gas production in a digester is often outcompeted by the gas consumption of an appliance and thus the gas supply pressure decreases over the use period. Because biogas is not used at the same rate at which it is produced, it must be stored somewhere. The gas must be efficiently transported from the digester to the storage tank to use if it is to be used in a simple, low-cost manner. To reduce the number of variables presented by biogas supplied from a bio

digester, the air compressor was used as a biogas storage as shown in the figure below. A small size compressor, which has a volume of 50 liters, can hold one and half-hour of the biogas used for cooking. The pressure of biogas fuel which is stored in the compressor will be regulated using a pressure regulator and the flow of the gas will be restricted using the one-way valve.

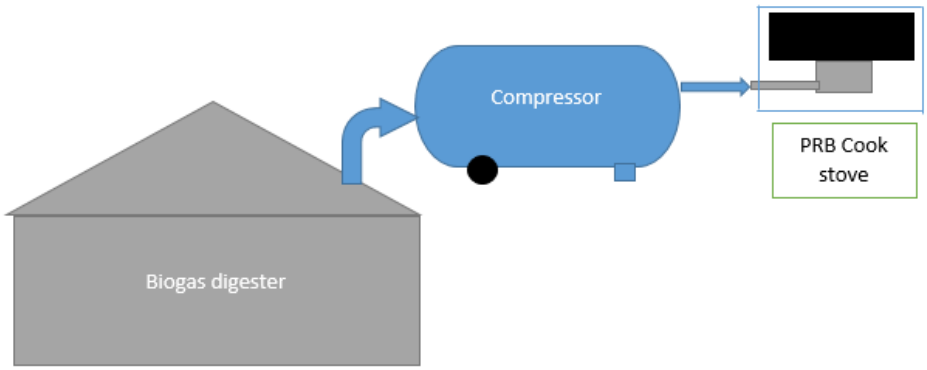

Figure 3-4 Compressing the biogas in to 50L tank

The mass flow rate was controlled and locked in at the set point through an iterative process. The difference in mass of the gas in the tire tube over some time was recorded and a mass flow rate was calculated. The flow of the gas is controlled by a one-way valve and measured by a flow meter, which has a range of 0-10 Liters per minute. For the baseline experiment, the mass flow rate of the biogas is set to be 0.0766 grams per second.

$$\dot{m} = \rho_{Biogas} \bullet \dot{V}_{Biogas}$$

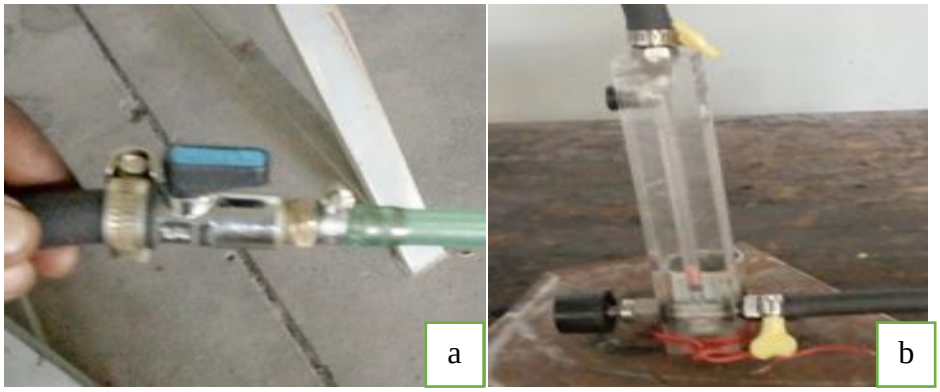

Figure 3-5 (a) One–way control valve and (b) Gas flow meter

The porous radiant burner (PRB) biogas stove prepared for experimental setup is shown in Figure 3-7. The burner consists of a two porous burners, a burner casing, and a mixing tube. The

downstream section of the burner called the preheating zone of the porous radiant burner is made of cat iron and the upstream section which is called the combustion zone is made of highly radiating and conducting Silicon Carbide (SiC).

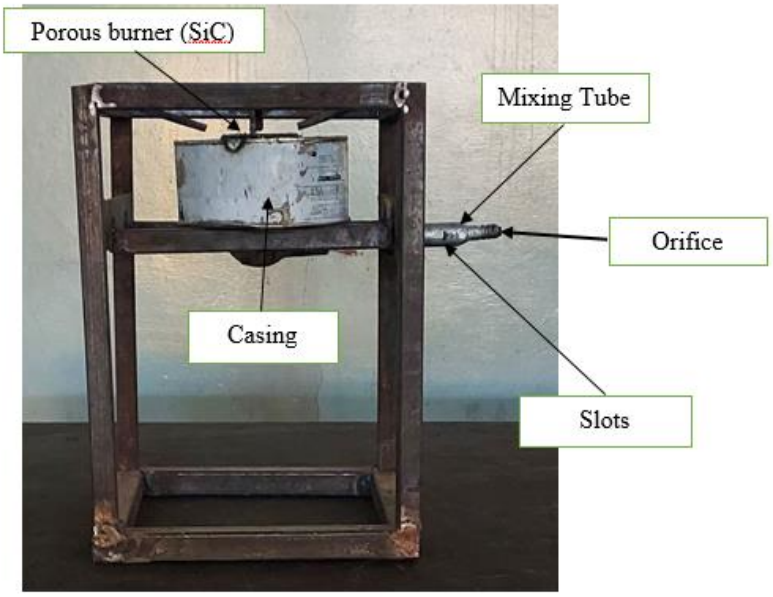

Figure 3-6 Self-aspirated domestic biogas stove with two-layer PRB

The biogas fuel is delivered from a pressurized compressor cylinder equipped with a pressure regulator to the mixing tube through a small aperture, and the air is provided using ports (slots) close to the fuel inlet. The flow rate of air and fuel will be adjusted to obtain the necessary equivalency ratio using a valve and will monitor by mass flow rate meters before entering to mixing chamber as shown in the schematic diagram of the experimental setup in Figure 3-7.

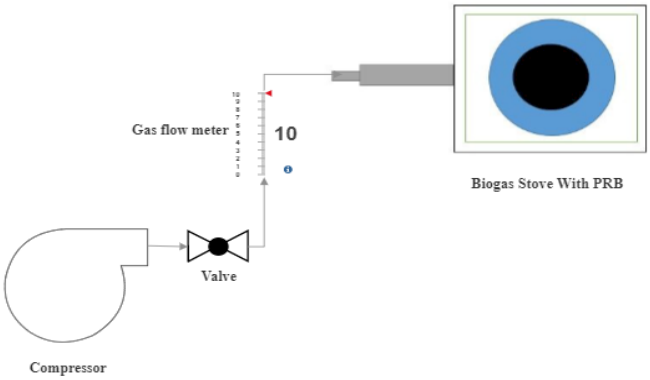

Figure 3-7 Schematic of Biogas cook stove experimental setup

To summarize the overall experimental setup, the biogas, which was stored in the compressor will, goes to the stove fuel inlet port passing through the pipe as shown in the experimental setup in the figure below. The one-way valve will be placed on the pipes between the compressor and the gas flow meter. This one-way valve is used to regulate the flow of the gas and the flow will be measured by the gas flow meter. Next to the gas flow meter, the pipe will be connected to the burner fuel inlet and the full will be going to the burner port and will be ready to ignite. The photographic view of the overall test setup is shown in the next figure 3-8.

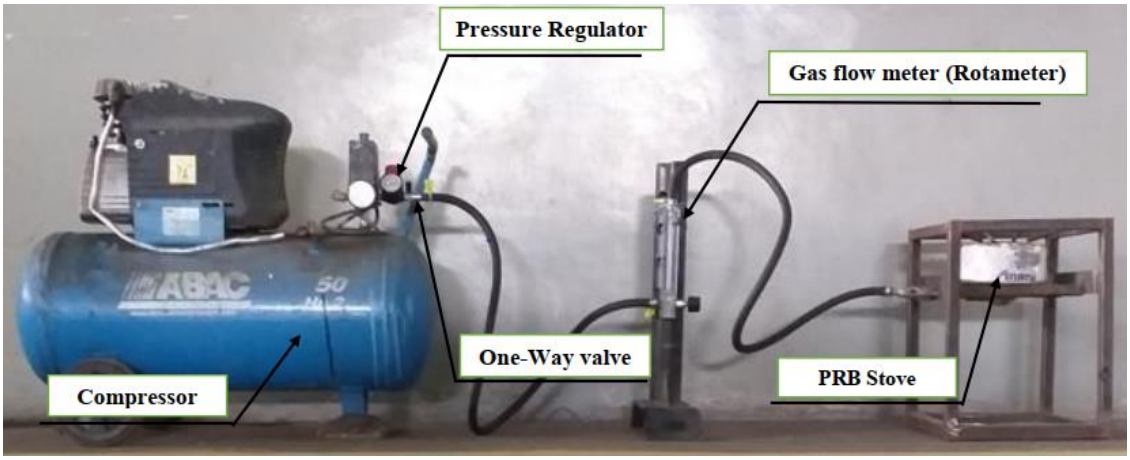

Figure 3-8 Photographic View of Experimental Setup

3.7.2 Test protocols

The experiments conducted to validate followed a water boiling test (WBT) protocol which is illustrated and mentioned in WBT version 4.2.3 of Clean Cookstoves (2014). Specifically, a 2.5-liter cold start test was used as the structure for the experiment. The test is termed cold start because the entire stove is at ambient temperature before the beginning of the test. The WBT protocol calls for temperature-controlled tests, or the duration of a test set by how long it takes to increase the temperature of 2.5 liters of water from 22 to boiling, or 94 ℃ (boiling temperature of water at the altitude of 1920m). This defined flow rate was termed a low firepower condition. Shorter, time-controlled tests are possible with gaseous burners due to a constant, linear change in water temperature over time. Thermal efficiency was defined as the energy delivered to a 3L pot of water divided by the total energy provided to the burner in the form of fuel. Thermal efficiency was a function of flame temperature and structure, pot dimensions, and distance from the burner to the pot. In this experiment, pot dimensions and distance from the burner to the pot were fixed.

The following steps outline the protocol for each test.

- The mass of a standard 3L pot was measured and recorded. 2.5 Kg of 22 ℃ water was added to the tared pot.
- The pot and water were moved on the pot supports of the burner. An immersed type the k-type thermocouple was inserted through a hole in the wood to the midpoint of the water column.
- The gas container was opened with the mass flow rate set at 0.0114 g/s (6 LPM) and ignited at the burner head.
- Keeping a constant flow rate, the temperature and flow control continued to record data as the water's temperature increased on the record sheet. At the five-minute mark, the water temperature was recorded.
- When the water starts to boil and the temperature remains constant, that point will be recorded as the boiling temperature of the water. The pot of water was immediately removed from the stove for mass measurement and comparison to the pre-test mass of the pot and water.
- Thermal efficiency was calculated from the results of the beginning water mass, change in water mass, change in water temperature, the time consumed to boil the water, and the biogas calorific value.

3.7.3 Performance Analysis of Biogas Stove

a) Thermal Efficiency Measurement

It is required to measure the temperature of the initial and final temperatures of the water as well as the ambient temperature in order to ascertain the thermal efficiency of the stove. The temperature of the water and the atmosphere were measured using the immersed thermometer as shown in Figure 3-9. In accordance with the instructions, a water-boiling test will be used to determine the porous radiant burner's thermal efficiency. The experiment's stirrer-equipped vessel will be chosen, and the weight of the filled vessel with water will be recorded. Once the flame has settled, the vessel will be maintained above the burner while the water's starting temperature is measured using a glass-mercury thermometer. Heating the water until it reaches the desired temperature.

(a) Self-aspirated PRB biogas stove (b) Conventional biogas stove

Figure 3-9 Photographic views of thermal efficiency measurement with WBT

The time taken to boil the water to its specified temperature will be noted and the thermal efficiency of the burner will be calculated using the following formula,

$$\eta_{thermal} = \frac{\left(m_{water} \times C_{p,water}\right)\left(T_{f,water} - T_{i,water}\right) + \left(\Delta m_{water} \times h_{e,water}\right)}{\dot{m}_{Biogas} \times t_{boil} \times Q_{LHV}} \quad (3\text{-}9)$$

Where m_w is water mass, c_w is the water specific heat, m_p is the pan mass, and c_p is the pan specific heat, $Q_{th} = m_f . Q_{LHV}$ is input thermal load, m_f is the mass of the fuel used during the experiment and Q_{LHV} is lower calorific value of biogas.

b) Surface Temperature distribution measurement

When the flame stabilizes, the thermocouples will be installed in the radial direction of the porous radiant burner as shown in Figure 3-10. A certain biogas flow rate was used to ignite the porous radiant burner at first, and then the airflow rate was gradually increased to reach the desired equivalency ratio. K-type thermocouples will be used to measure the temperature distribution throughout the burner's axial distance, and a data acquisition device will be used to record the results. Thermocouples will be installed at predetermined intervals along the burner's surface to measure the temperature distribution along the burner. Utilizing an immersed temperature measuring instrument, the burner's surface temperature will be determined.

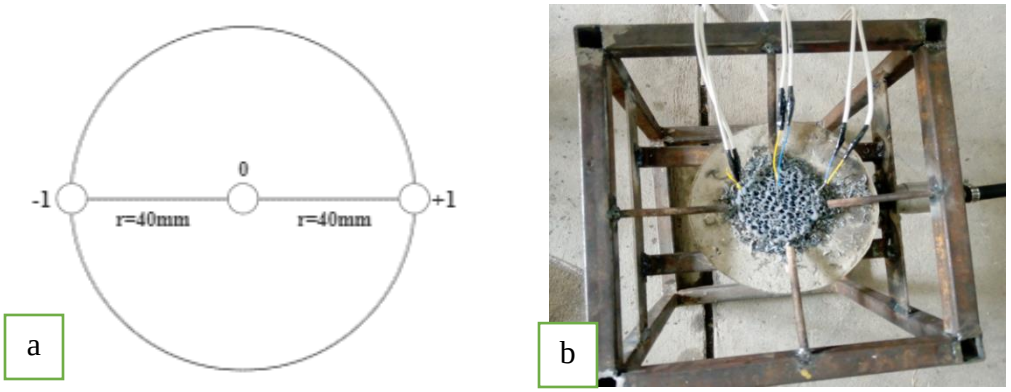

Figure 3-10 Thermocouple: (a) schematic diagram showing radial positions and (b) Picture of location

c) Emission measurement

A flue gas sensor analyzer through a sampling hood as shown in the schematic diagram of Figure 3-11 measures the gaseous emissions produced by the combustion of biogas in a own aspiration household stove with a porous burner. The flue gas analyzer was user-calibrated using predetermined calibration gases before the experiment. The flue gases from a biogas porous radiant burner were all gathered inside an enclosed hood placed at the top of the stove and it has a gas outlet at the top to efficiently absorb the full emissions stream.

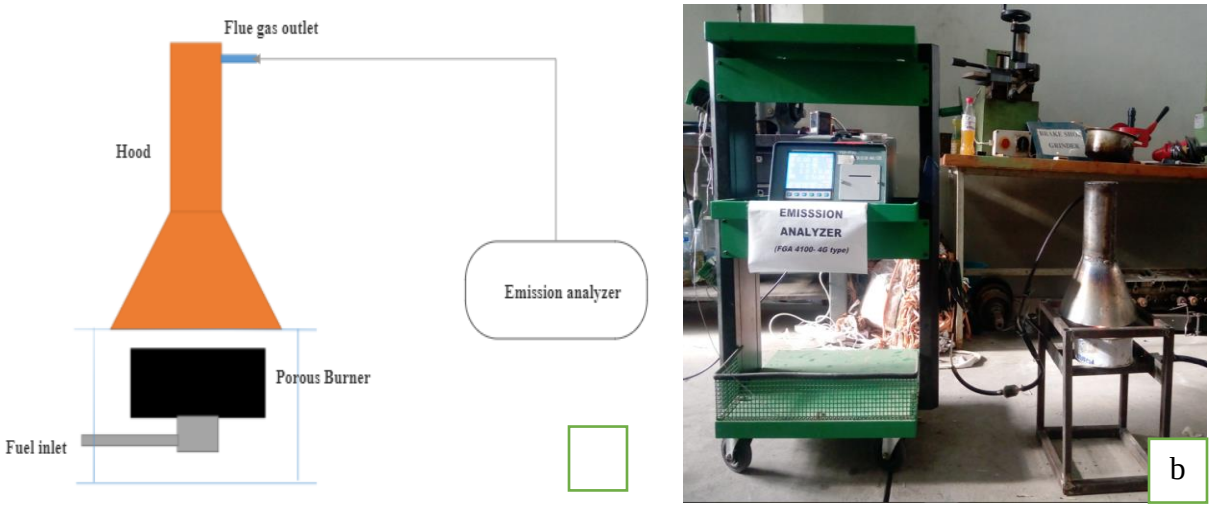

Figure 3-11 (a) Schematic diagram and (b) photographic view of the emission measurement setup

As illustrated in Figure 3.11, the sensor of the analyzer will be linked to the flue gas outlet, drawing the emissions stream from the hood into a collecting and analysis system. Carbon monoxide (CO), and NOx were the substances of interest. Data on carbon monoxide and nitric oxide (NOx) were reported in parts per million (ppm) and percent, respectively. Methane is the sole hydrocarbon found in biogas in appreciable amounts, according to flue gas analyzer measurements of total NOx and CO. The procedure for measuring the gas compounds and converting them into a uniform mass flow is described in the steps that follow.

Before the test, a five-minute background was recorded for all three compounds of interest, and start the combustion. A test was started after the combustion flame is stabilized and concentrations (ppm and %) of the three gas compounds were recorded by the emission analyzer. After all these experiments have been done repeatedly, the results will be recorded well and, that will be analyzed and discussed further in the next chapter.

CHAPTER 4

RESULT AND DISCUSSION

Following CFD analysis, quantitative findings are shown below for the distributions of static pressure, velocity magnitude, total pressure, turbulent kinetic energy, and dynamic viscosity. When the burner axis and fuel inlet pipe radius are utilized for the cross-section, all figures have a contour map on the cross-sectional surface.

4.1 Result of CFD Analysis

4.1.1 Grid Independence Test

The mesh size and cell count are determined by the size of the elements and the number of nodes used to discretize the flow domain, and the mesh size has an impact on the CFD results. Typically, a grid independence test is performed to ensure that the CFD output is independent of the mesh size. The best way to save calculation time is to run this test on the chosen model rather than all results, which would be computationally expensive. The measurement points are chosen and assigned to the burner surface as shown in the figure to record the results in remote locations of the burner. The burner surface contains all nine measuring locations, which are utilized to gauge pressure, turbulence energy, and velocity magnitude. The simulation record variables have the maximum and minimum values through the simulation iteration. The grid-independent test will use the average value over the iteration as a comparison parameter.

The self-aspirated PRB model with an orifice diameter of 1.2 mm, slot length and width of 25 and 15 mm is chosen for the grid independence test, and in this analysis, an equivalence ratio of 0.9 is given. According to Figure 4-1, the parameters are assessed at the PRB's outlet portion, which is where points 7, 8, and 9 are positioned (at the outlet section of the burner). The grid creation is originally set up using automatic mesh generation, and in this case, the number of divisions was increased five times to increase the number of analysis components to execute the grid independence test. Elements steadily increase in quantity from 8609 to the finer number of 48849. Figure 4.1 presents the measuring points, and the comparison of pressure, velocity, and turbulent kinetic energy with the number of elements. The CFD result of the grid independence test is estimated by the root mean square error of the parameters through the change in the number of divisions

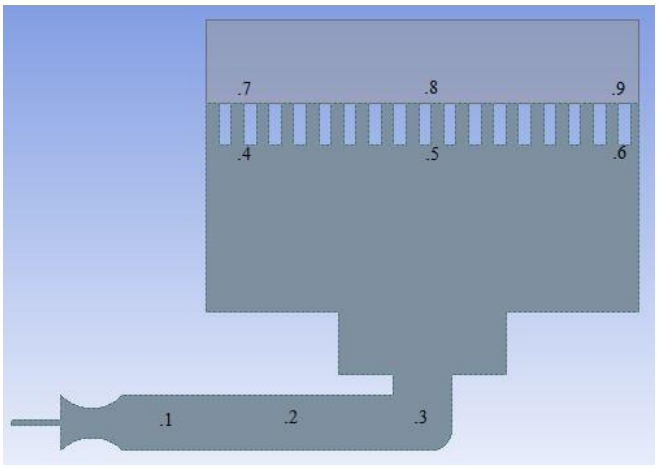

(a) Measurement points

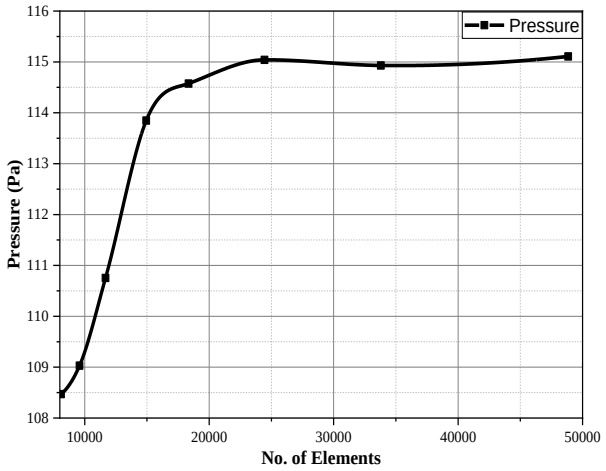

(b) Number of Element Vs Pressure

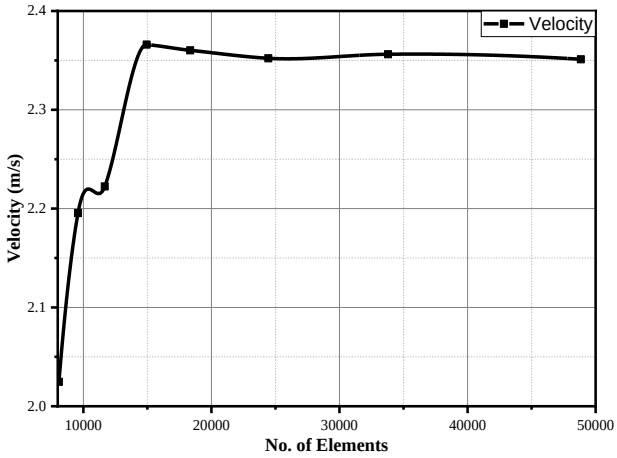

(c) Number of Element Vs Velocity

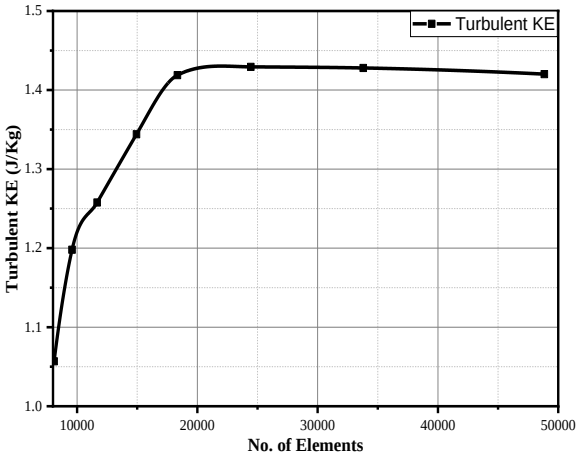

(d) Number of Element Vs Turbulent KE

Figure 4-1 Grid Independence Test

The divergence of the pressure, velocity, and turbulent kinetic energy values while the number of elements is growing is depicted in Figure 4.1(a), (b), and (c). Calculating the RMSE of the parameters at each increment point of the number of elements is important to determine the point or number of elements at which the values of pressure, velocity, and turbulent energy will converge. In the first three modifications in the number of items, the parameters' values deviate by more than 10% according to the test. The RMSE values for pressure, velocity, and turbulent kinetic energy are 0.00187, 0.004165, and 0.004886, respectively, during the last two modifications in the number of elements. Less than 10% makes up the RMSE values at the most recent two changes in element

number. According to the examination of grid independence, there is less pressure, velocity, and turbulent kinetic energy deviation on the burner's output section without a noticeable grid dependency. The study of the remaining burner models will move forward using the number of elements (48849) based on the results from the aforementioned results. The purpose of this study is to evaluate the impact of orifices and slots on the process of creating a self-aspirated PRB stove. To look into the choice of three different self-aspirated PRBs and a burner model with the current PRB. As a result, the findings of pressure, velocity, and turbulent kinetic energy for the chosen burner models are shown in this section.

4.1.2 Static and Total Pressure

With inlet mass flow rates of biogas and air of 0.0746 and 0.433 Kg/s with self-aspirating PRB burners operating at typical atmospheric conditions and for forced air supply PRB with the same flow rate as self aspirated but at different pressure level which is 200 KPa, Figure 4-2 shows the static and total pressure color mapped for the baseline and self-aspirated PRB burner models. According to a visual examination of the color-mapped results, the static pressure in a pipe flow often achieves its highest values close to solid borders. The combustion zone, which is the upper part of the burner in this case, is porous, and when utilizing a burner with a forced air supply, the lowest static pressure value is observed there. The maximum static pressure is found at the fuel inlet pipe because the inlet flow is perpendicular to the burner surface, forcing flow to build up on the burner and not transverse the porous zone. Pressure decreases as one travels into the preheating and combustion zones. Self-aspirated burners, which have an air inlet port and an intake orifice, exhibit the same pattern. However, in the porous zone, the pressure decrease is a little less pronounced.

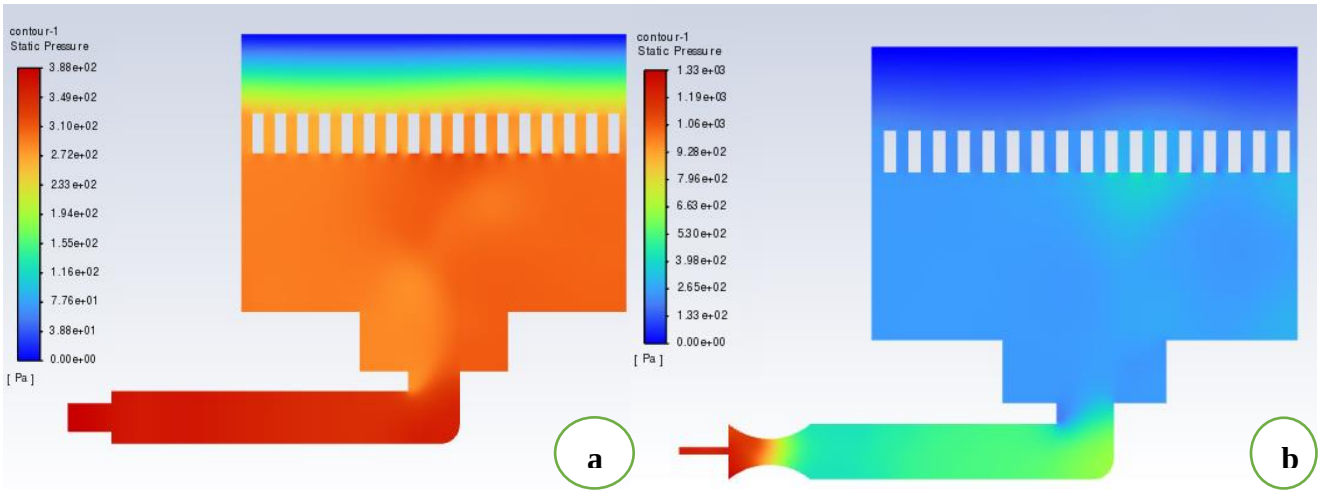

Static pressure of Baseline model (Forced air supply) Static pressure of self-aspirated burner (Case 1)

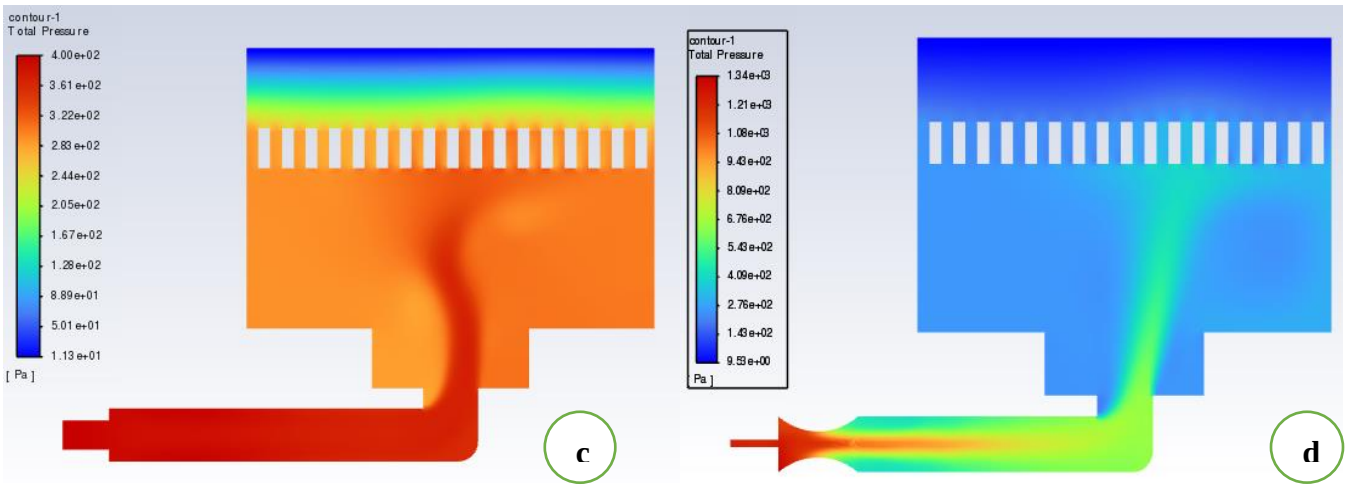

Total pressure of the Baseline model (Forced air supply) Total pressure of the self-aspirated burner (Case 1)

Figure 4-2 Color-mapped results of static and total pressure

The statistical parameters can be used to locate the measurement locations' pressure. The pressure readings of each measurement point for all burner models are shown in Figure 4.2. It is assumed that pressure rises at the entrance zone, where point 1 is located, and starts to reduce in the preheating zone, based on the results of the static pressure measurements at the measurement sites. All burner models have an increase in pressure drop in the combustion zone, but the base line model in particular experiences a greater increase in pressure drop because its pressure is higher than the others but the pressure drop is higher than the other models. The remaining self-aspirated burner models have the same trend as the baseline model but the pressure drop at measurement points 7, 8, and 9 is lower than the baseline model.

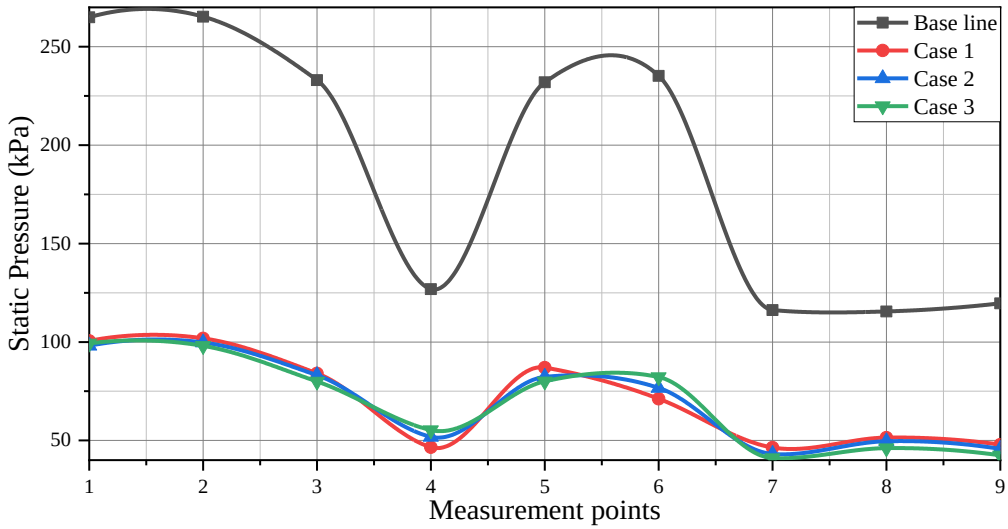

Figure 4-3 Comparison of pressure values of different burner models

This result implies that a very low-pressure drop is caused by a fuel and air entry orifice and slot at the porous material. Even so, the flow rate seems low since the combustion zone is not significantly entered until after a static pressure, level is reached and the flow in the mixing chamber increases. Faster flow rates would lead to greater static pressure measurements and a quicker transition into the combustion zone. The need for additional, highly pressurized air supplies to allow the fuel to pass through the dimensions of porosity on the interface surface between the preheating and combustion zones is the main contributing factor to the flow accumulation in the burner mixing chamber for forced air supply.

4.1.3 Velocity Magnitude Distribution

Figure 4-4 shows the distribution of velocity magnitude for the self-aspirated PRB (case 1) burner model and the baseline (forced air supply) model. By deducting the static pressure from the total pressure, one may get the dynamic pressure. In this regard, the velocity distribution can be examined and estimated using the static and total pressure distribution figures. The magnitude of the velocity is relatively low where static pressure acquires bigger values because the kinetic energy is converted into potential energy as static pressure and compresses the local domain in a region of denser gas. It is also discovered that the entrance pipe and the passageway connecting the preheating and combustion zones are flow-resisting regions. The speed is decreased and the static pressure is raised by this flow resistance.

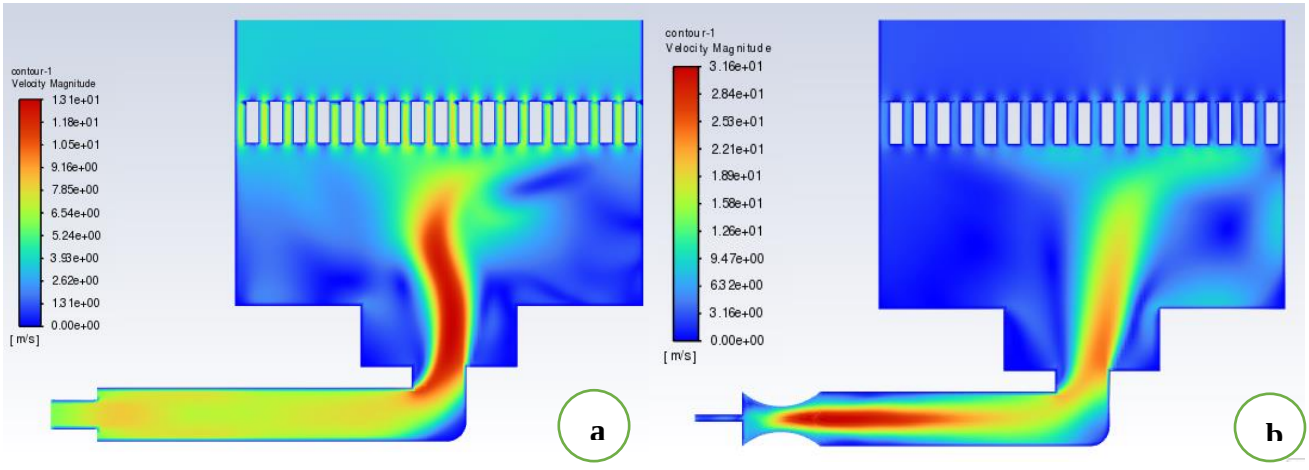

Baseline (Forced air supply) Self-Aspirated PRB (Case 1)

Figure 4-4 Color mapped result of velocity magnitude profiles

It can be seen that the solid boundaries of the porous burner core aid in retaining the majority of the flow energy. The flow then intensifies near the mixing chamber's top and, in the case of a burner with a forced air supply, starts to resemble stagnation. The porous interface surface reduces the mixture of fuel and air's speed after it leaves the mixing tube because it acts as a medium to maintain the flow laminar. The fuel flow, however, in the case of a self-aspirated burner develops in the intake pipe toward the direction of the mixing chamber, develops in the entrance of the PZ, and goes through the CZ as a result of the orifice and slots. The velocity magnitude map, which shows a slight increase in flow rate approaching the combustion zone in the upper portion, further supports the statement made in the static pressure map. It is also clear that a lot of flow energy is expended at the surface where the inner and outer volumes converge.

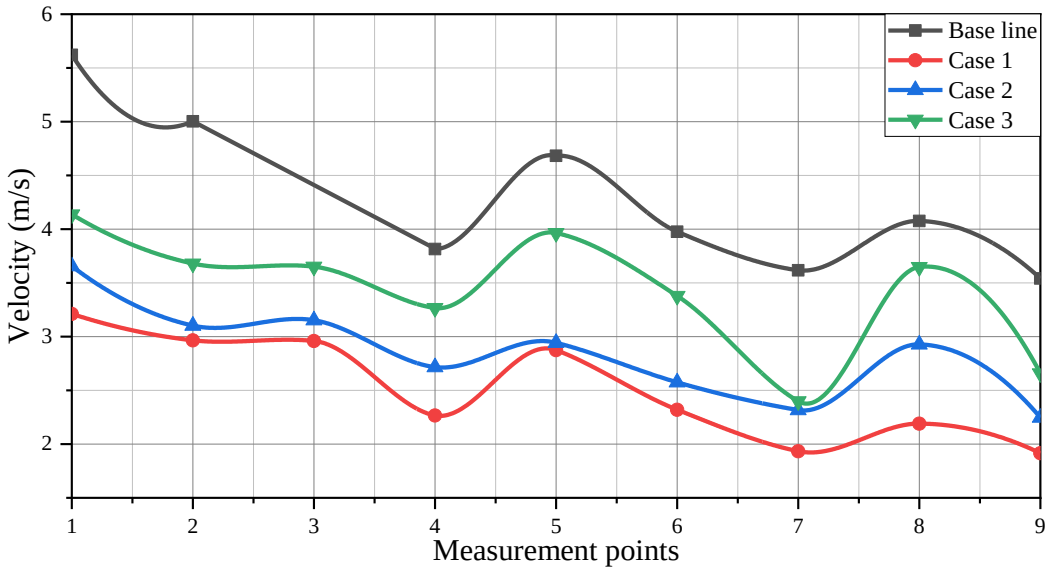

Figure 4-5 Comparison of velocity magnitude of different burner models

The magnitude of the velocity at each of the measurement points for each burner model is shown in Figure 4-5. When compared to other self-aspirated burner models, the baseline (forced air supply) burner model has a maximum velocity at point 8 of 4.697735 m/s, which is significantly higher than the other burner models. At the inlet or mixing tube, all burners have roughly the same velocity. However, after the combustion zone, the velocity of the fuel air mixture for all model starts to decline. Burner model 3 has better velocity values of 2.59 m/s, 3.64 m/s, and 2.658 m/s at measurement sites 7, 8, and 9 in the combustion zone when compared to the self-aspirated burner models. The other two self-aspirated burner models show a similar trend as case 3, by having lower velocity than the baseline

model. However, the values of this burner model are slightly lower than the self-aspirated burner model 3.

4.1.4 Turbulent Kinetic Energy

Based on the provided equivalence ratio, the turbulent kinetic energy for the base burner model and the three self-aspirated PRB models is examined. The color-mapped profile of the baseline (forced air supply) and self-aspirated PRB (case 1) turbulent kinetic energy is shown in Figure 4-6. As would be expected, boundary effects and nearby mixing cause turbulence to form at measurement points 4, 5, and 6 in the case of the baseline model at the interface between the preheating and combustion zone and walls and at measurement points 2 and 3 in the case of the self aspirated burner models at the connecting area between mixing tube and burner port.

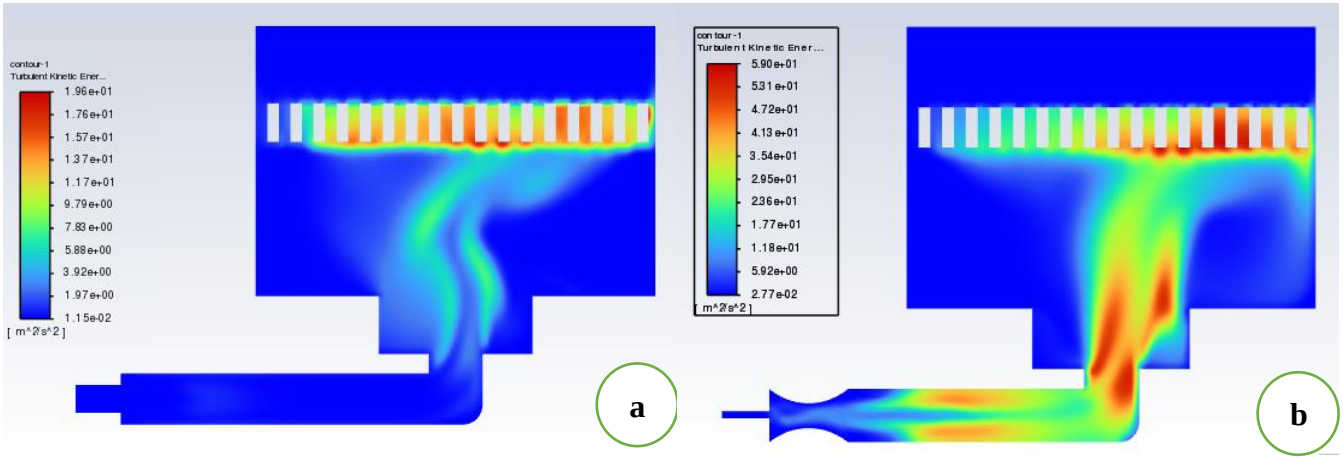

Baseline model (Forced air supply) self-aspirated burner (Case 1)

Figure 4-6 Color-mapped Turbulent kinetic energy contours

According to the color-mapped results, the maximum amount of turbulent kinetic energy is around 4.7816 J/Kg for self-aspirated burners and 3.690942 J/Kg for forced air supply burners. The increase in total enthalpy is included in the 6 J/kg of energy recovered from the flow. With a forced air supply burner, a sizable portion of the energy is lost because of turbulence, followed by self-aspiration and further heat loss. The total pressure map may also support a decrease in flow energy. Nonetheless, turbulence is anticipated in this situation to aid in gas mixing. The level of turbulence and combustion efficiency can be related in the context of future gas mixing. In terms of mixing and combustion efficiency, the self-aspirated porous radiant burner thus surpasses the forced air supply burner.

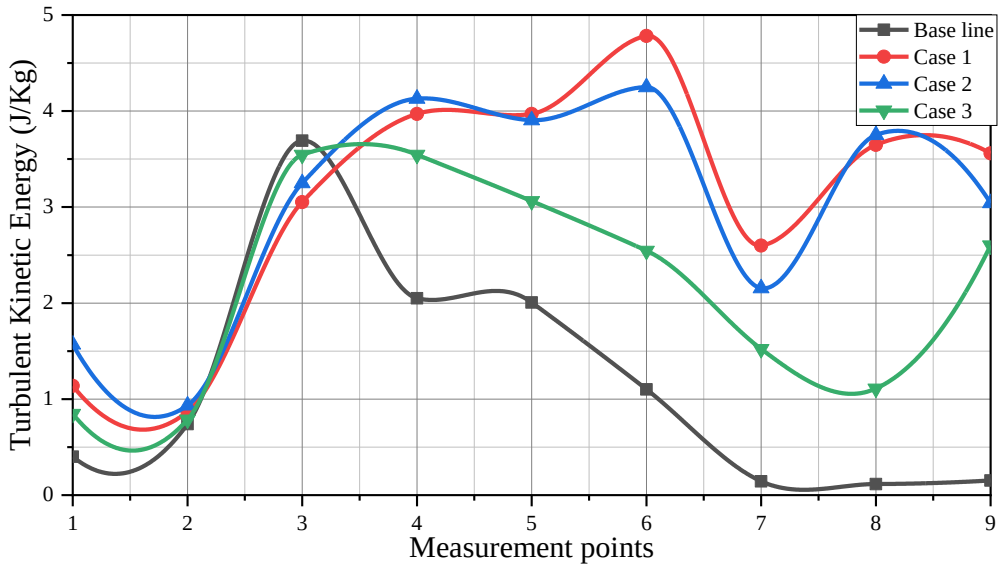

Figure 4-7 Comparison of Turbulent KE of different burner models

The comparison of the turbulent kinetic energy between the baseline and self-aspirated burner models is shown in Figure 4-7. According to the results of the turbulent kinetic energy, the measurement points from 2 to 7 for all burners had the highest turbulent kinetic energy. Since the base burner model has more turbulent kinetic energy than the other burner models, there is roughly zero energy in measurement points 7 to 9 at the location of the combustion zone. The turbulent kinetic energy of the other three self-aspirated burner models is lower than that of the baseline burner model. In comparison to the other two self-aspirated burner models, burner model 3 has the lowest turbulent kinetic energy (1030 J/kg), and burner model 1 has the most (4.781 J/kg).

4.2 Discussion on CFD Results

The examination of several burner models, utilizing the current baseline (forced air supply) PRB as the reference benchmark to assess the performance of the self-aspirated burner models, is described in the aforementioned section. To describe the impact of orifice and slot in self-aspirated PRB models, three new burner models are proposed in this paper, each with a distinct equivalency ratio. Three alternative examples were created by combining the orifice and slot geometry of the PRB burner to explore this phenomenon. This section will explain the simulation's findings concerning the pressure, velocity, and turbulent kinetic energy that develop inside the burner as a result of the effects of the orifice and slot.

The burner pressure profile at the inlet and outlet section for each burner is grouped to explore the role that orifice and slots play in minimizing the pressure drop that is produced in the burner models. One model set contains two pressure values with the same equivalence ratio that corresponds to the burner's intake and exit. Because the baseline (forced air supply) model has a higher pressure of 264.43491 KPa at the burner's inlet, the fuel-air mixture cannot cross to the porous material and accumulates in the preheating zone, and all of the pressure built in the inlet section drops to 98.511 kPa. As a result, there is a significant pressure drop in the inlet section. Due to this characteristic, the burner is known as a forced air supply. A compressor is used to raise the pressure and circulate the fuel/air combination in the burner. The orifice and slots in the self-aspirated PRB models keep the pressure in the combustion zone from decreasing and keep the fuel/air mixture from building up in the preheating zone. Nonetheless, there will be sufficient pressure to allow passage across the porous combustion zone. Figure 4-8 shows the pressure value at the entrance and outlet for the self-aspirated PRB model.

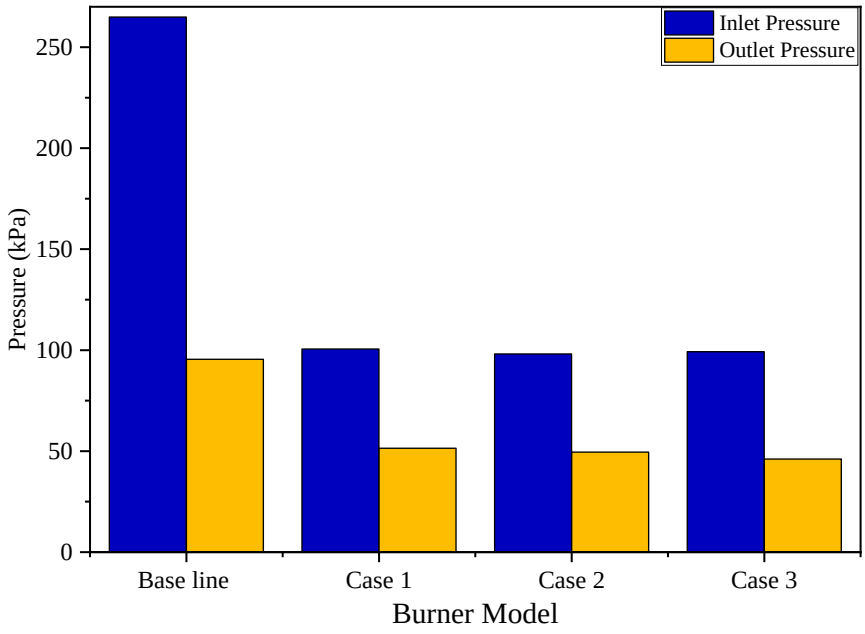

Figure 4-8. The effect of the orifice and slot on the Inlet and outlet pressure of the burner

As can be seen in the image, the self-aspirated PRB models have sufficient pressure to allow the fuel-air mixture to cross the boundary between the preheating and combustion zones. The self-aspirated PRB model 2 has the highest pressure at the burner's outlet out of these three variants. The burner type 2 has a slot length of 20mm and an orifice diameter of 1mm. As the fuel-air combination is

increased, the pressure rises proportionately. Although the pressure at the burner's output is a little lower in the other two self-aspirated PRB models than it is in case 3, both models follow the same general trend. With the self-aspirated burner models, the effect of the orifice and slot reduces the inlet pressure and converts that pressure into the burner's output section. Based on this finding, the self-aspirated PRB model 3 performs better in terms of minimizing the pressure drop.

As discussed concerning the impact of orifices and slots on burner pressure, the burner inlet mixing tube's orifices and slots will also have an impact on velocity. Figure 4-9 plots the velocity at the intake and output of the burner to show how the orifice affects the mixture of fuel and air's speed. According to the figure, all burner models are constructed with a higher velocity at the burner's inlet, with the base model having the greatest velocity of 5.62233 m/s. By using a self-aspirated PRB model 1, the lowest velocity is created at the burner's inlet. The basic thing here is not developing the velocity at the inlet of the burner, but it is important that deliver the fuel-air mixture with high velocity to the combustion zone where the fuel-air mixture is burned.

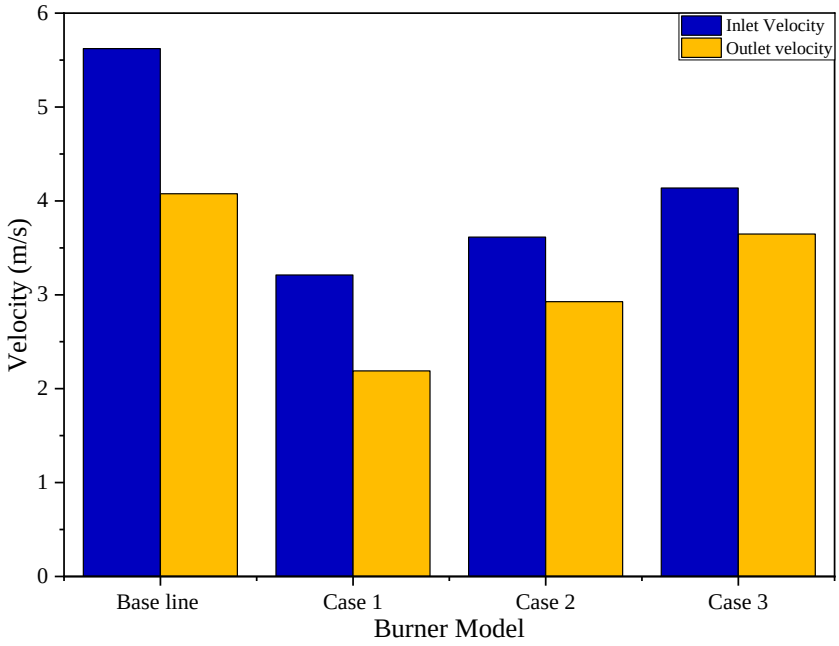

Figure 4-9 The effect of the orifice and slot on the Inlet and outlet velocity of the burner

Figure 4-10 demonstrates that all of the burners have a higher velocity at the burner's inlet. The velocity at the burner's exit is crucial, as was previously stated. According to this analysis, the greatest velocities for the self-aspirated PRB models are 2.18925 m/s, 2.92753 m/s, and 3.64673 m/s for

burner models 1, 2, and 3, respectively. The self-aspirated PRB model 3 has a better outlet velocity that is utilized to move the fuel-air combination to the combustion zone and can perform better than the other self-aspirated PRB models depending on the burner's velocity.

All burners experience fluctuations in flow velocity or turbulent kinetic energy from the mixing tube to the burner port as a result of turbulent kinetic energy. The fuel-air mixture does not reach the combustion zone due to higher turbulence energy created in the burner, and the base PRB model has to convert the flow velocity to heat due to turbulence in the previously described region. The self-aspirated PRB models' ability to reduce the turbulent kinetic energy was significantly impacted by the inclusion of orifices and slots. The kinetic turbulence energy in these burners is lower than the kinetic turbulence energy in the PRB model's baseline. From this self-aspirated PRB model, model 3 has a lower tendency of fluctuation of flow velocity or turbulent kinetic energy.

4.3 Result and Discussion on Experimental Investigation

4.3.1 Thermal Efficiency

The PRB's thermal efficiency measurement is shown in Figure 4.6 along with the biogas flow rate. The thermal efficiency increases for a certain flow rate of biogas and then drops as the fuel flow rate increases. Such behavior is brought on by richer conditions, which allow the flame front to move as a result of increased fuel flow rates, leading to the greatest release of volumetric heat. The lowest flow rate among the biogas flow rates examined produces the most efficiency. For a biogas flow rate of 6 LPM, the highest efficiency of 61% was attained in the case of forced air supply PRB, and 59% thermal efficiency is obtained in the case of self aspirated PRB. Similar to this, a flow rate of 8 LPM results in minimal efficiency of 53% and 51% being attained in the case of forced air supply and self-aspirated PRB biogas cook stoves. Figure 4.10 compares the thermal efficiency of a standard biogas cook stove, forced air supply and self-aspirated porous radiant burners. The porous radiant burner operating in a fuel-rich environment is chosen for comparison since the conventional cook stove is built for conditions where fuel is abundant. The traditional cook stove's thermal efficiency was between 54 and 46% when the biogas flow rate was between 6 and 8 LPM, whereas the self-aspirated porous radiant burner's efficiency was between 59 and 51% which is 2% lower than the cook stove manufactured by Kaushik et al. (2021) . The thermal efficiency data makes it evident that the porous radiant burner's improvement in thermal efficiency is between 6 and 16%.

The thermal efficiency, which is achieved in the case of forced air supply porous radiant burner developed by Kaushik et al. (2021) is range from 54-61% corresponding to the biogas flow rate of 240-480 L/hr and equivalence ratio of 0.9. Though the burner performs with better surface temperature distribution and lower pollutant emission discussed in the later sections. From the figure, depending on the results of the thermal efficiency, the self-aspirated PRB stove is slightly lower than the stove working with forced air supply system but it performs better than the conventional burner biogas cook stoves.

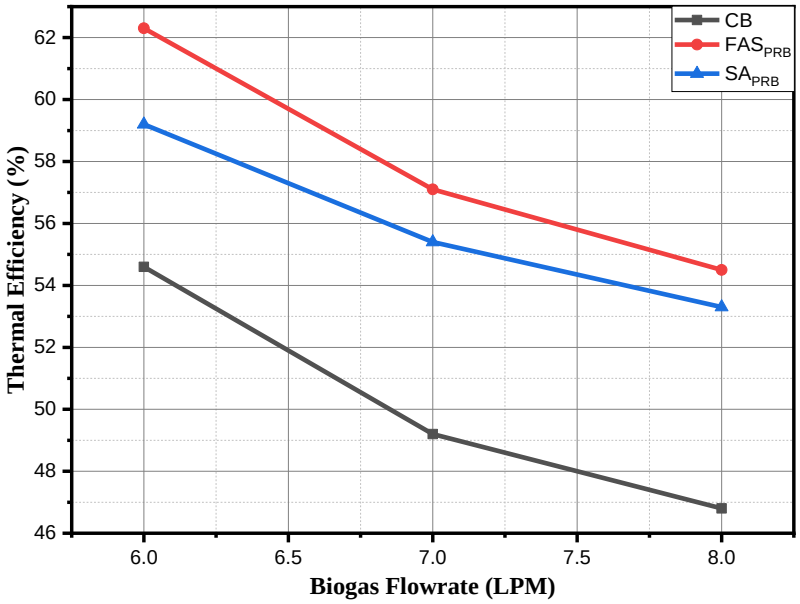

Figure 4-10 Thermal efficiency comparison for conventional and PRB cook stove

The efficiency of conventional biogas cook stoves decreases with an increase in biogas flow rate, and the decline is greater than that of the porous radiant burner. The cause of this behavior is related to the fact that when the flow rate increases, the highest point of the flame rises, increasing convective heat loss. Because of the coupled effect of the radiative and convective circulation of the heat of highly emissive porous substances for the entire enclosure, the porous radiant burner operates better in terms of thermal efficiency than conventional cook stoves. Since the adoption of a porous radiant burner for residential cooking.

4.3.2 Surface Temperature Distribution

Figure 4.11 displays the porous radiant burner surface temperature distribution for various biogas flow rates. The trend of the highest possible surface temperature of the porous radiant burner is shown

by the biogas flow rate increment. The primary factor generating such heat distribution is the environment's exposure to loss of heat by radiation and conduction from the burner casing. The air-fuel combination experiences less flow resistance in the center of the burner than it does in the area close to the burner's periphery because of the burner casing. For a biogas rate of flow of 8 LPM, the largest temperature differential between the center and the periphery was 59 °C. Lower surface temperature differences between the center and the periphery of the porous radiant burner are caused by lowering the biogas flow rate to increase optimum mixing with the air. To compare the surface temperature distribution between the self-aspirated and forced air supply PRB stove figure 4.11 presents. Figure 4-11 shows the surface temperature distribution (a) self-aspirated PRB and (b) forced air supply PRB. From the figure shows that, the self-aspirated PRB has lower surface temperature distribution than the forced air supply PRB corresponding to the biogas flowrate. The temperature difference between the center and the periphery of the burner in the case of the forced air supply is 42℃, which is lower than the temperature difference existed in the self-aspirated PRB. A richer mixture and a greater temperature difference between the burner's center and edges result from a higher biogas flow rate. Additionally, because the mixing zone temperature is lower than the biogas's self ignition point (650 ℃), there was little chance that a flame flashback would develop. Other biogas flow rate data exhibit a comparable trend, although the temperature values decreased as the biogas flow rate increased, which is understandable given the drop in heat input.

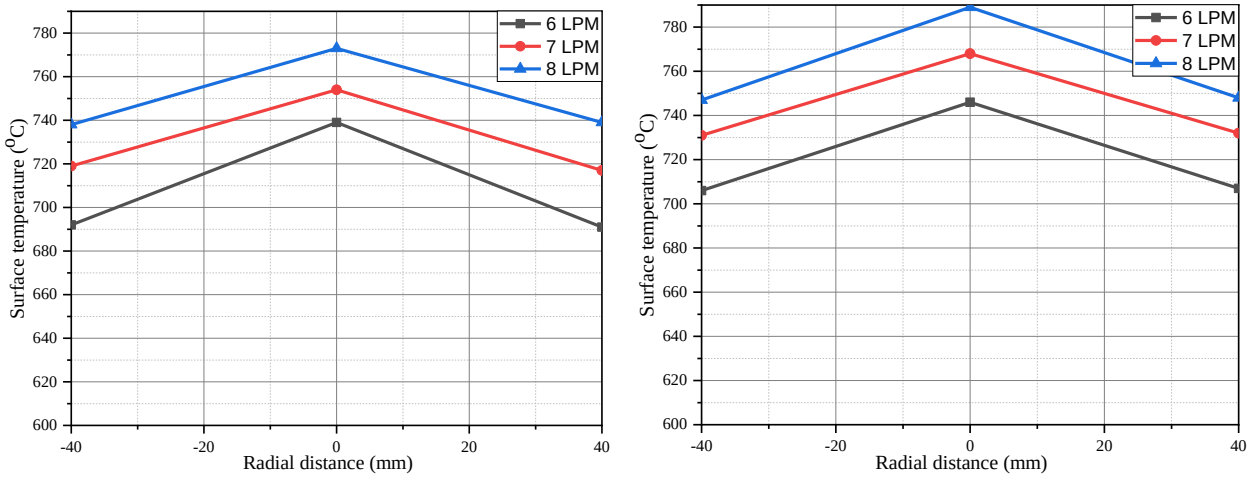

(a) Self-Aspirated PRB (b) Forced air supply PRB

Figure 4-11 Surface temperature distribution of PRB in the radial direction

4.3.3 Emission Measurement

A consequence of the burner's exhaust gas's close proximity to the user, the measurement of CO and NOX emissions is crucial because the porous radiant burner has been investigated for household cooking applications. All emission values used in the current analysis are collected on a dry basis with an adjustment of 3% oxygen level. Figure 4-12 shows the impact of flow rate of biogas on emissions of CO and NOx for conventional burner, forced air supply and self-aspirated PRB cook stoves. Similar to thermal efficiency, a 6-8 LPM flow rate is used for porous radiant burners when comparing emission levels with the conventional biogas burners. Figure 4.8 illustrates the comparison of NOx and CO levels between a traditional cook stove with forced air supply and self-aspirated porous radiant burners.

In a self-aspirated porous radiant burner, measured CO and NOx levels ranged from 41 to 55 ppm and 4 to 10 ppm, over the full spectrum of fuel flow rates. As the same as for forced air supply porous radiant burner biogas fueled stove the CO and NOx values are ranges from 35 to 43 and 2 to 4 ppm for the corresponding biogas flowrate. As opposed to the traditional burner, where the same values were 235-257 and 9-14 ppm. In both self-aspirated and forced air supply porous radiant burner, as the biogas flow rate increases, CO and NOx emissions rise as well. This is because as the biogas flow rate rises, fuel movement slows down, reducing the rate at which the air and fuel are mixed, and increasing emissions. Shortened time spent in the porous matrix, which results in more unburned CO, is the other factor contributing to the highest CO emission.

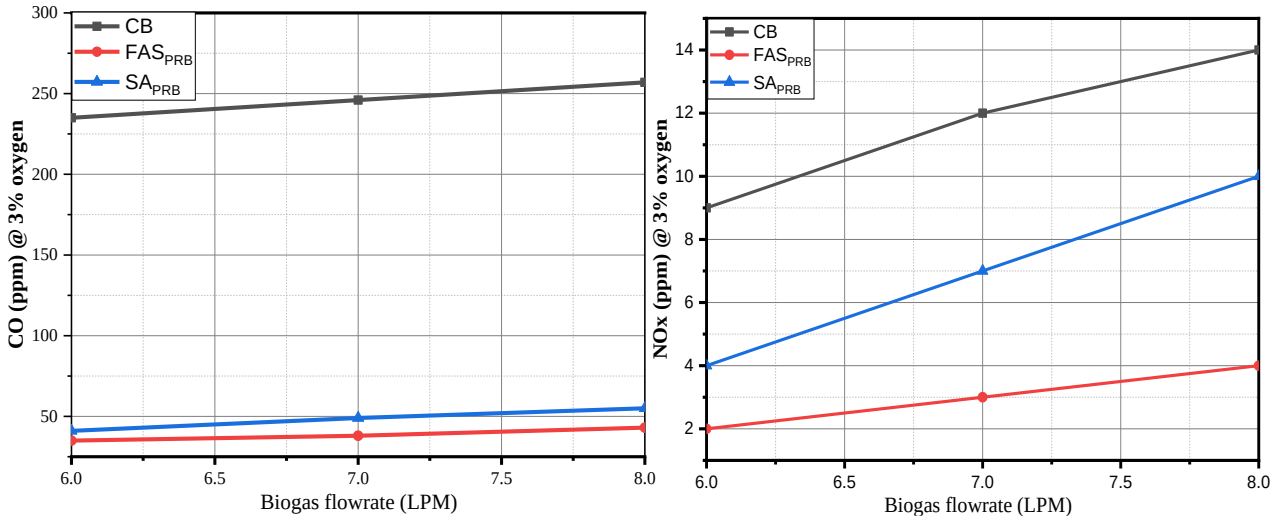

Figure 4-12 Comparison of conventional burner with PRB CO and NOx emissions

The NOX emission is a major factor in self-aspirated porous radiant burners, and it will get worse as the flow rate rises and the temperature rises. Since NOx concentration solely depends on the equivalency ratio for NOx concentration to reach a trace level, Figure 4.8 illustrates the effect of fuel flow rate on NOx emission. As the figure shows the equivalence ratio for the self-aspirated PRB were limited due to the air enters to the slots naturally and the equivalence ratio is reduce, the NOx values are becomes higher than the forced air supply PRB. The figure shows that for both the standard biogas cook stove and the porous radiant burner, CO and NOx emissions rise as the biogas flow rate rises. Because of better combustion and longer residence times, measured CO and emissions from porous radiant burners are lower than those from typical biogas cook stoves. Similarly, it was discovered that the porous radiant burner's NOx emission was far lower than that of a traditional cook stove. Lower NOx emission results from the burner's lower surface temperature in the porous radiant burner. High temperature in the reaction zone causes increased NOx from conventional cook stove burners because of fuel-rich combustion (interface between preheating and combustion zone). According to the aforementioned experiment into biogas, combustion in radiant pores burners operating in the 6–8 LPM flow range, stable functioning takes place. The forced air supply porous radiant burner can reduce CO and NOx emissions by 83.3 % and 41.9% compared to conventional biogas burners, and the self-aspirated PRB cook stove emits lower CO and NOx emissions by 79.4 % and 28.4% than the conventional burner respectively. Forced air supply PRB increased thermal efficiency by up to 5%, and self-aspirated PRB enhance the thermal efficiency by 3% higher than the conventional burner biogas stove. Self-aspirated porous radiant burner's overall performance shows that it can take the place of a traditional cook stove.

CHAPTER 5

CONCLUSION AND RECOMMENDATION

5.1 Conclusion

Cooking process is one of the greatest consumers of renewable and non-renewable energy sources and potential contributor to air pollution. Using conventional biogas burner working with free flame combustion for cooking is an old technology that reduces the thermal efficiency of burner and leads to incomplete combustion. Because of these factors, the conventional biogas cook stove burner becomes less efficient and emits harmful pollutants into the atmosphere. To solve the aforementioned issue, numerous studies have been conducted to increase thermal efficiency and decrease pollutant emissions by substituting the current traditional biogas cook stove with a porous radiant burner. Air compressors were used in conjunction with the newly developed porous radiant burner to overcome the pressure drop and increase the fuel-air mixture's velocity because the burner's porosity resulted in a higher-pressure drop and lower velocity of the inlet biogas fuel and air mixture passing through the porous material. The newly created porous radiant biogas burner does not proceed beyond the experimental test to residential application depending on these considerations. Through computational fluid dynamics and experimental research, the challenge of producing porous radiant burner-aided cook stoves is addressed in this thesis. Here, CFD analysis is used to choose the optimal design concept for a self-aspirated PRB cook burner that is portable and suitable for usage in both urban and rural households.

A numerical model that has been created represents the species transfer that takes place within and between the solid and fluid phases of a porous burner. ANSYS FLUENT 2021 was used to model the burner as a "porous zone" using distinct solid and fluid energy equations. To overcome the pressure drop and enhance the velocity of the intake fuel-air mixture used to build a self-aspirated PRB cook stove, the main goal is to study the flow parameters of the present PRB and add some features to it, such as orifice and slots. Details of the porous media and its assembly that is intended for use as a burner are included in the geometry for the CFD study. The so-called porous metal matrix burner's planned application operational parameters were taken into consideration when choosing the boundary conditions. On this basis, the fluid's density and the distribution of static and total pressure, velocity profiles, and turbulent kinetic energy were assessed. According to the CFD results, static pressure and velocity distribution reach their maximum at the center of the PRB

and the mixture passes through the porous owing to the orifice as the inlet flow direction is perpendicular to the flange surface. Because of this profile, the PRB has a very low-pressure drop, which results in a low need for pumping power, achieving the goal of building a self-aspirated PRB cook stove.

For a comparative comparison, biogas combustion tests have been performed on a newly constructed self-aspirated Porous Radiant Burner (PRB) and a commercially available Conventional Burner (CB). The current work investigates the thermal efficiency and pollutant emission of both burners during combustion. From the experimental results, it is obtained that the highest thermal efficiency possible of the Self-aspirated PRB stove was 59-51% and with the conventional burner, it is from 46-54% with the corresponding flow rate of 6-8LPM. Concerning gas flow rate and within the stable working range, emission monitoring has been done using a range of wattages. The values for CO and NOx concentrations for self-aspirated PRB stoves were determined to be in the range of 41 to 55 ppm, and 4 and 10 ppm, respectively, at gas flow rates of 6 and 8 LPM. These results show that the self-aspirated domestic cook stove with PRB produces cleaner combustion than its equivalent, which produced substantially higher readings of 235 to 257 ppm and 9 to 14 ppm, respectively. Results indicate that when compared to a domestic biogas cook stove with a conventional burner, the PRB powered by biogas emits up to a maximum of 79.4% and 28.4% less CO and NOx, respectively. As the flow rate of biogas increased, both CO and NOx showed a rising trend. In the case of NOx, changes in flow rate and equivalence ratio had a bigger effect than changes in heat load. The PRB biogas cook stove with self-aspiration has also been shown to be more effective in terms of combustion. Depending on all the factors discussed in the above section, here it is concluded that, the self-aspirated PRB biogas domestic cook stove performs slightly lower than the forced air supply PRB domestic cook stove, but it performs higher than the conventional burner biogas cook stove.

5.2 Recommendation and Future Works

The self-aspirated residential biogas a two-layer porous radiant burner on a cook stove underwent experimental study and computational fluid dynamics to improve thermal efficiency while lowering pollutant emissions from the existing traditional biogas cook stove. More investigations may be undertaken in the future for further advancement based on the current research. According to the findings, it is advised that cast iron and ceramic foam be utilized as the burner materials for

a two-layer porous radiant heater. Cast iron material must be replaced with a better thermally resistant ceramic material to increase the burner's durability. For a better use of these self-aspirated PRB stove, it is strongly recommended to weight the biogas fuel, which comes from the digester until its pressure reaches more than one bar. The current study focuses on the study in the construction of a home biogas stove that is self-aspirated and has a porous radiant burner, and the following scopes for future study on the creation of porous burners.

- ✓ Detailed performance investigation on developing self-aspirated PRB biogas cook stove
- ✓ Construct a thorough life cycle study and assess the efficiency of a newly created PRB cook stove for household use.
- ✓ PRB cook stove thermal efficiency is being further improved, and geometrical parameters are being optimized.

Reference

Abdulkarim, A. H., Ates, A., Altinisik, K., & Canli, E. (2019). Internal flow analysis of a porous burner via CFD. *International Journal of Numerical Methods for Heat & Fluid Flow*.

Awulu, J., Iyidiobu, B., & Ugbede, J. (2020). COOKING PERFORMANCE OF A DEVELOPED BIOGAS BURNER (STOVE). *International Journal of Engineering Applied Sciences and Technology, 4*(12), 11-16.

Balmes, J. R. (2019). Household air pollution from domestic combustion of solid fuels and health. *Journal of Allergy and Clinical Immunology, 143*(6), 1979-1987.

Bank, W. (2018). *Global Economic Prospects, January 2018: Broad-Based Upturn, but for How Long?* : The World Bank.

Belino, M., Bosshard, H., Chen, S., Custodio, M., Lopena, J., Meris, P., & Saccuan, E. (2015). Development of efficient and cleaner charcoal stoves for cooking applications in a rural residential dwelling. *Proceedings APCBE*.

Berko, E. (2018). *Design, Construction and Assessment of an Improved Hybrid Charcoal-LPG Cookstove.* University of Ghana.

Beyene, G., Kumie, A., Edwards, R., & Troncoso, K. (2018). *Opportunities for transition to clean household energy in Ethiopia: application of the household energy assessment rapid tool (HEART)* (9241514493). Retrieved from

Bharathiraja, B., Sudharsana, T., Jayamuthunagai, J., Praveenkumar, R., Chozhavendhan, S., & Iyyappan, J. (2018). Biogas production–A review on composition, fuel properties, feed stock and principles of anaerobic digestion. *Renewable and Sustainable Energy Reviews, 90*(April), 570-582.

Bildirici, M., & Özaksoy, F. (2018). An analysis of biomass consumption and economic growth in transition countries. *Economic research-Ekonomska istraživanja, 31*(1), 386-405.

Bott, L. (2014). *Controlled Cooking Test*. SNV.

Bryden, M., Still, D., Scott, P., Hoffa, G., Ogle, D., Bailis, R., & Goyer, K. (2005). *Design principals for wood burning cook stoves*: Aprovecho Research Center.

Castro, A., Calvo, A., Blanco-Alegre, C., Oduber, F., Alves, C., Coz, E., Amato, F., Querol, X., & Fraile, R. (2018). Impact of the wood combustion in an open fireplace on the air

quality of a living room: Estimation of the respirable fraction. *Science of the Total Environment, 628*, 169-176.

Cookstoves, G. A. f. C. (2014). The water boiling test version 4.2. 3: GACC Washington, DC, USA.

Cozzi, L., Gould, T., Bouckart, S., Crow, D., Kim, T., Mcglade, C., Olejarnik, P., Wanner, B., & Wetzel, D. (2020). World Energy Outlook 2020. *Paris: IEA*.

Demissie, S. W., Ramayya, V. A., & Nega, D. T. (2016). Design, fabrication and testing of biogas stove for 'Areke'distillation: the case of Arsi Negele, Ethiopia, targeting reduction of fuelwood dependence. *International Journal of Engineering Research, 5*(03).

Devi, S., Sahoo, N., & Muthukumar, P. (2019). Combustion of biogas in Porous Radiant Burner: low emission combustion. *Energy Procedia, 158*, 1116-1121.

El-Mahallawy, F., & Habik, S.-D. (2002). *Fundamentals and technology of combustion*: Elsevier.

Eriksson, O. (2010). Environmental technology assessment of natural gas compared to biogas. *Natural Gas, 1*, 127-147.

Ethiopia, S. (2019). *Biogas Dissemination Scale-Up Programme (NBPE+) Report of Bio-digester Users' Survey (BUS)*. Retrieved from Addis Ababa, Ethiopia:

Forn, E. B., Kamp, L., & Kroesen, O. (2014). Analysis of the development of domestic biogas in Ethiopia. *Unpublished masters thesis, faculty of technology, policy and management, Delfit University*.

Harris, G. L. (1995). *Properties of silicon carbide*. Washington DC, USA: Iet.

Herrera, B., Cacua, K., & Olmos-Villalba, L. (2015). Combustion stability and thermal efficiency in a porous media burner for LPG cooking in the food industry using Al2O3 particles coming from grinding wastes. *Applied Thermal Engineering, 91*, 1127-1133.

Huang, K., Li, W., Xie, B., Rao, P., Peng, C., Chen, D., & Wu, J. (2011). Preparation and mechanical properties of Al2O3/Al laminated ceramic matrix composites. *Journal of Wuhan University of Technology-Mater. Sci. Ed., 26*(5), 891-896.

International, W. *CLEAN AND EFFICIENT COOKING TECHNOLOGIES AND FUELS*. Retrieved from USA:

Ismail, A., Ibrahim, N., Shamsuddin, K., Abdullah, M., & Zubair, M. (2018). *A practical approach in porous medium combustion for domestic application: A review*. Paper presented at the IOP Conference Series: Materials Science and Engineering.

Ismail, A. K., Abdullah, M. Z., Zubair, M., Ahmad, Z. A., Jamaludin, A. R., Mustafa, K. F., & Abdullah, M. N. (2013). Application of porous medium burner with micro cogeneration system. *Energy, 50*, 131-142.

Jia, Z., Ye, Q., Wang, H., Li, H., & Shi, S. (2018). Numerical simulation of a new porous medium burner with two sections and double decks. *Processes, 6*(10), 185.

Jugjai, S., & Sanitjai, S. (2007). Parametric studies of thermal efficiency in a proposed porous radiant recirculated burner (PRRB): a design concept for the future burner. *International Energy Journal, 18*(2).

Kang, S., Choi, J. Y., & Choi, S. (2019). Mechanism of heat transfer through porous media of inorganic intumescent coating in cone calorimeter testing. *Polymers, 11*(2), 221.

Kaushik, L. K. (2019). *Performance and feasibility assessment of porous radiant burner aided cook-stoves for LPG, biogas and waste cooking oil fuels.* (Degree of Philosophy), Indian Institute of Technology, Gowatti, Gowatti, India.

Kaushik, L. K., Mahalingam, A. K., & Palanisamy, M. (2021). Performance analysis of a biogas operated porous radiant burner for domestic cooking application. *Environmental Science and Pollution Research, 28*(10), 12168-12177.

Kaushik, L. K., & Muthukumar, P. (2019). Performance assessment of a porous radiant cook stove fueled with blend of waste vegetable oil (WVO) and kerosene. *Energy Procedia, 158*, 2391-2396.

Kebede, D., & Kiflu, A. (2014). Design of Biogas stove for injera baking application. *International Journal of Novel Research in Engineering and Science, 1*(1), 6-21.

Keles, S., Bilgen, S., & Kaygusuz, K. (2017). Biomass energy source in developing countries. *Journal of Engineering Research and Applied Science, 6*(1), 566-576.

Leta, B. (2009). National survey on current status of institutional biogas systems installed in Ethiopia. *Horn of Africa Regional Environment Center/Network, Addis Ababa University, GTZ-German Technical Cooperation–Ethiopia*.

Lombardi, F., Riva, F., Bonamini, G., Barbieri, J., & Colombo, E. (2017). Laboratory protocols for testing of Improved Cooking Stoves (ICSs): A review of state-of-the-art and further developments. *Biomass and bioenergy*, *98*, 321-335.

Malico, I., & Mujeebu, M. A. (2015). Potential of porous media combustion technology for household applications. *International Research Establishment for Energy and Environment (IREEE)*.

Marchese, A. (2015). Chemical Equilibrium Course Pack. *Combustion*.

Mishra, N. K., & Muthukumar, P. (2018). Development and testing of energy efficient and environment friendly porous radiant burner operating on liquefied petroleum gas. *Applied Thermal Engineering*, *129*, 482-489.

Mujeebu, M. A., Abdullah, M. Z., Bakar, M. A., Mohamad, A., & Abdullah, M. (2009). Applications of porous media combustion technology–a review. *Applied energy*, *86*(9), 1365-1375.

Mujeebu, M. A., Abdullah, M. Z., Bakar, M. Z., Mohamad, A. A., Muhad, R. M., & Abdullah, M. K. (2009). Combustion in porous media and its applications--a comprehensive survey. *J Environ Manage*, *90*(8), 2287-2312. doi:10.1016/j.jenvman.2008.10.009

Mulugeta, B., Demissie, S. W., & Nega, D. T. (2017). Design, optimization and CFD simulation of improved biogas burner for 'Injera'baking in Ethiopia. *nternational Journal of Engineering Research & Technology*, *6*(1).

Orhorhoro, E., Oyejide, J., & Abubakar, S. (2018). Design and construction of an improved biogas stove. *Arid Zone Journal of Engineering, Technology and Environment*, *14*(3), 325-335.

Pantangi, V., Kumar, A. K., Mishra, S. C., & Sahoo, N. (2007). Performance analysis of domestic LPG cooking stoves with porous media. *International Energy Journal*, *8*(2).

Pantangi, V., Mishra, S. C., Muthukumar, P., & Reddy, R. (2011). Studies on porous radiant burners for LPG (liquefied petroleum gas) cooking applications. *Energy*, *36*(10), 6074-6080.

Petro, L. M., Machunda, R., Tumbo, S., & Kivevele, T. (2020). Theoretical and Experimental Performance Analysis of a Novel Domestic Biogas Burner. *Journal of Energy*, *2020*.

Pradhan, P., Mishra, P. C., & Samantaray, B. B. (2018). Performance and emission analysis of a novel porous radiant burner for domestic cooking application. *Heat Transfer Engineering*, *39*(9), 784-793.

Raja, I. A., & Wazir, S. (2017). Biogas production: the fundamental processes. *PakistanCattlekit, Mohlin Lal, Pakistan: COMSATS Institute of Information Technology*.

Samoilenko, M. (2018). *Design of porous medium burners by means of additive manufacturing.* École de technologie supérieure.

Sawyerr, N., Trois, C., Workneh, T., & Okudoh, V. I. (2019). An overview of biogas production: fundamentals, applications and future research. *International Journal of Energy Economics and Policy*.

Sime, G., Tilahun, G., & Kebede, M. (2020). Assessment of biomass energy use pattern and biogas technology domestication programme in Ethiopia. *African Journal of Science, Technology, Innovation and Development, 12*(6), 747-757.

Soma, D. M., Chhabra, S., & Sehgal, S. (2018). CFD Analysis of Porous Medium Burner for Domestic Cooking Application. *Indian Journal of Science and Technology, 11*(26), 1-7.

Tajebe, L. (2016). Bio-Gas Technology Adoption in Rural Ethiopia: It's Effect on the Crisis of Deforestation. *Journal of Energy Technologies and Policy*.

Tierney, C., Wood, S., Harris, A. T., & Fletcher, D. F. (2009). *Computational Fluid Dynamics Modelling Of Porous Burners.* Paper presented at the Seventh International Conference on CFD in the Minerals and Process Industries CSIRO, Melbourne, Australia.

Zain, M. M., & Mohamed, A. R. (2018). An overview on conversion technologies to produce value added products from CH4 and CO2 as major biogas constituents. *Renewable and Sustainable Energy Reviews, 98*, 56-63.

Zeng, W., Liu, J., Ma, H., Liu, Y., & Liu, A. (2018). Experimental study on the flame propagation and laminar combustion characteristics of landfill gas. *Energy*, *158*, 437-448.

Ziabasharhagh, M., & Mohammadi, A. (2012). Numerical Simulation of Combustion in Porous Media. *Numerical Simulation–From Theory to Industry*.

APPENDIX

I. Mixing simulation background calculation

To validate the velocity estimate produced by ANSYS Fluent®, additional parameters were derived using the equivalency ratio determined in the mixing simulation. What happened was as follows:

1. Percent of the Stoichiometric Air was calculated from the equivalence ratio

$$\%\ of\ Stoich\ air = \frac{100}{phi}$$

2. Fraction of air needed to meet stoichiometric mixing before combustion

$$A\ stoich = \left[\frac{1\ mole\ of\ C\ in\ biogas}{1\ mole\ of\ C\ in\ methane} + \frac{2.4\ moles\ of\ H\ in\ biogas}{4\ moles\ of\ H\ in\ methane}\right] - \left[\frac{0.8\ mole\ of\ O\ in\ biogas}{2\ mole\ of\ O\ in\ Oxygen}\right]$$

3. Fraction of actual air entrained

$$a = \%\ of\ Stoich\ air * \frac{a\ stoich}{100}$$

4. Number of moles of air entrained per mole of fuel provided

$$\frac{Moles\ of\ Air}{Moles\ of\ Fuel} = 4.76 * a$$

5. The mole fractions of the air and fuel

$$Mole\ fraction\ of\ air = \frac{mole\ of\ air\ entertained}{moles\ of\ air\ entertained + 1\ mole\ of\ fuel\ provided}$$

$$Mole\ fraction\ of\ fuel = \frac{mole\ of\ fuel\ entertained}{moles\ of\ air\ entertained + 1\ mole\ of\ fuel\ provided}$$

6. Now that the bulk flow composition is understood, the volumetric flow rates of fuel and air can be calculated via the continuity equation

$$\dot{V}_{fuel}[LPM] = A_{XS,\,fuelinlet}[cm^2] \times v_{inlet}[\frac{cm}{s}] \times \frac{60s}{1\min} \times \frac{1L}{1000cm^3}$$

$$\dot{V}_{air}[LPM] = \text{mole fraction of air}\frac{\dot{V}_{fuel}[LPM]}{moles\ fraction\ of\ fuel}$$

7. Using biogas and air density, the mass flow rate can be calculated

$$\dot{m}_{fuel}\left[\frac{kg}{s}\right] = \dot{V}_{fuel}[LPM] * \frac{60\sec}{1\min} * \rho_{biogas}[\frac{kg}{s}] * \frac{1m^3}{1000L}$$

$$\dot{m}_{air}\left[\frac{kg}{s}\right] = \dot{V}_{air}[LPM] * \frac{60\sec}{1\min} * \rho_{air}[\frac{kg}{s}] * \frac{1m^3}{1000L}$$

II. Table of datasheet

1. Radial temperature distribution

Burner Type	Biogas Flow rate (LPM)	The temperature at Radial Position (°C)		
		-40mm	0	+40mm
Forced air supply PRB	6	706	746	707
	7	731	768	732
	8	747	789	748
Self-Aspirated PRB	6	697	739	694
	7	726	761	723
	8	731	783	724

2. Thermal Efficiency

Biogas Flow rate (LPM)	Thermal Efficiency (%)		
	CB	FAS_{PRB}	SA_{PRB}
6	54	61	59
7	49	57	54
8	46	53	51

3. Emission

Biogas Flow rate (LPM)	CO (ppm)			NOx (ppm)		
	CB	FAS_{PRB}	SA_{PRB}	CB	FAS_{PRB}	SA_{PRB}
6	235		38	9	3	4
7	246		41	12	5	7
8	257		46	14	8	10

III. Photographs in Developing and Testing PRB Cook-stove

1. Measurement of Thermal efficiency

2. Measurement of Surface temperature distribution

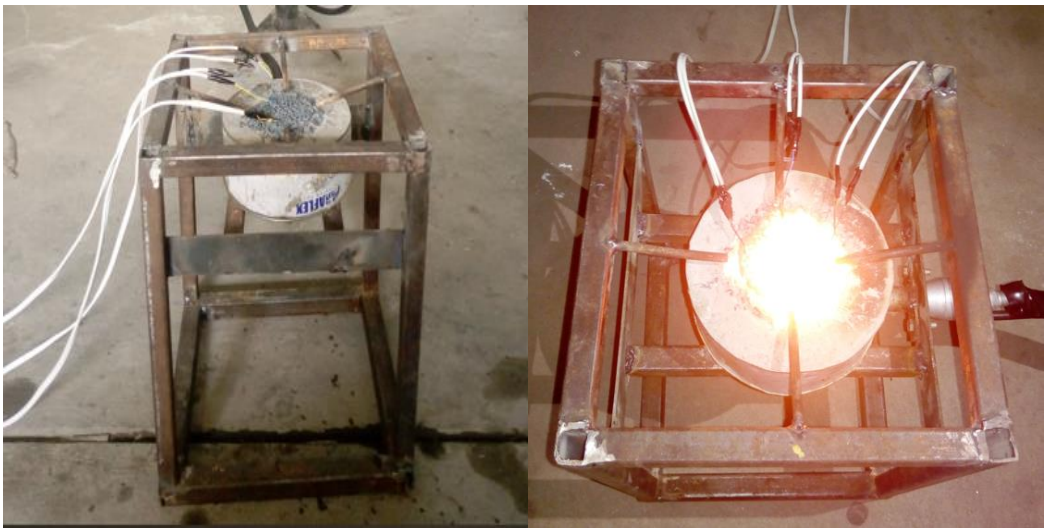

IV. Technical Information for Experimental Equipment

1. Pressure Gauge

Made	Warre instruments
Dial size	10mm
Readability	0.05 bar
Range	0-5bar
Accuracy	±0.05% full scale
Temperature limits	0℃ to 120℃

2. Compressor

Made	Ingersoll Rand
Item type	Reciprocating
Max. Pressure	16 Bar
Stage	2 stage
Tanker volume	50 Liters
Accessories	Outlet pressure regulator, air filter

3. Thermocouples

Make	Selec Digital Temperature Controller
Model	TC-303AX
Type of input	Metal sheathed K-type
Junction	Grounded
Range	-199 ℃ - 999 ℃
Accuracy	for K-type 0.25%

4. Thermometer

Make	Midloce
Model	NR-1900 Bimetallic analog thermometer
Configuration	Insertion
Application	Hot water
Max. Range	120 ℃

5. Mass flow rate meter

Type	ABR 19 Acrylic body rotameter
Make	VESKELER Instruments
Flow range	0 to 50 LPM
Flow accuracy	±0.35% of the full scale
Sensitivity	0.0001 L
Temperature range	-10 to 60 ℃
Operating pressure ranges	from 0 to 50 bar

6. Gas Analyzer

Manufacturer	Foshen Instruments
Item Model no.	FGA-4100
NO	0-3000 ppm
Error (Accuracy)	±5 ppm
Resolution	3 ppm
CO	0-10000 ppm
Error (Accuracy)	±10ppm
Resolution	3 ppm
O_2	0-25 Vol%
Resolution	0.1 Vol%
Error (Accuracy)	±0.2 Vol%